10/11-27-89 DSCW

# SANDIA REPORT

SAND89—0917 • UC—600
Unlimited Release
Printed October 1989

# Shock-Wave Characterization of Energetic Booster-Rocket Propellant WAK-2 and Its Simulant UGS

L. J. Weirick

**Prepared by**
**Sandia National Laboratories**
**Albuquerque, New Mexico 87185 and Livermore, California 94550**
**for the United States Department of Energy**
**under Contract DE-AC04-76DP00789**



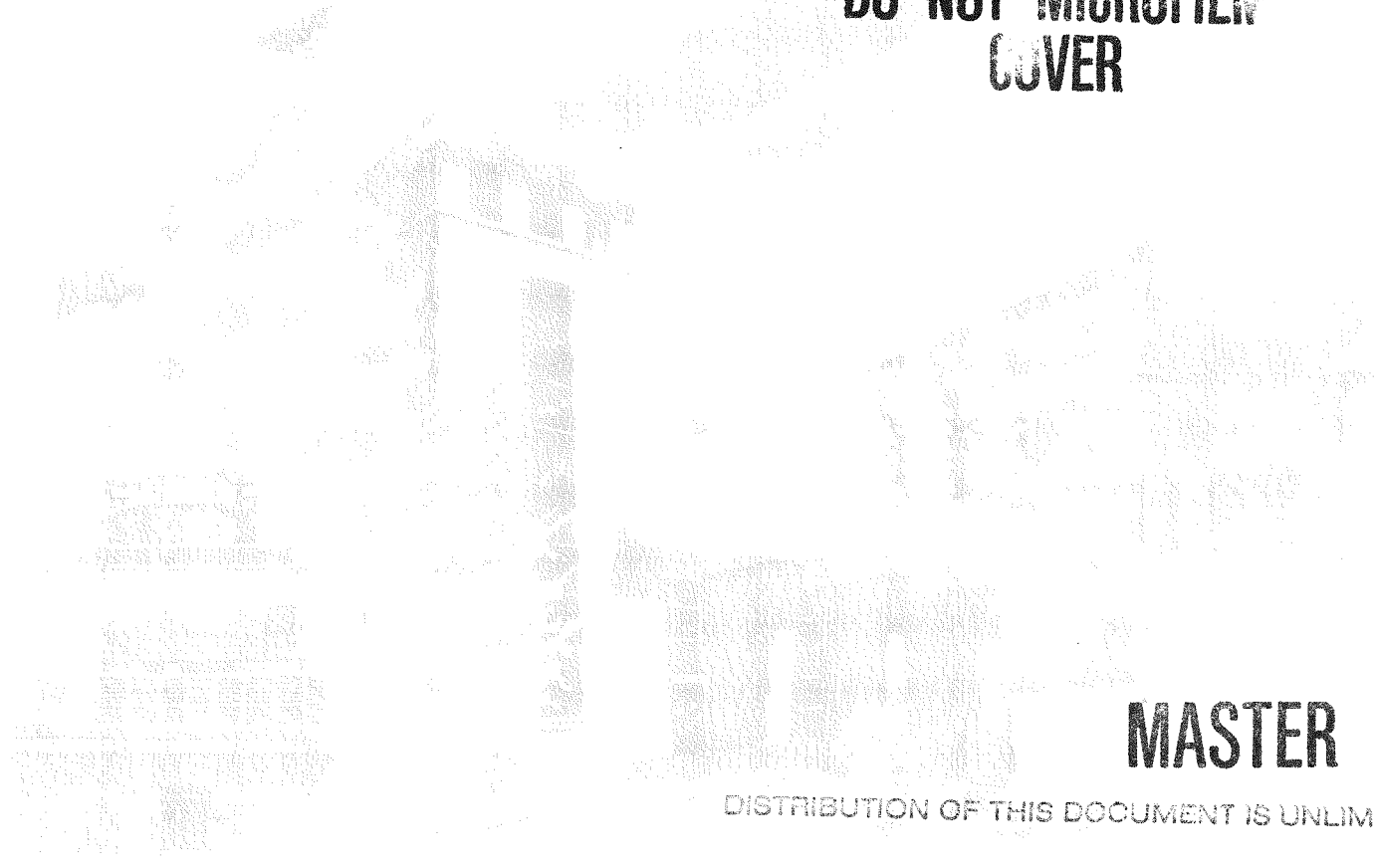

Issued by Sandia National Laboratories, operated for the United States Department of Energy by Sandia Corporation.



Available to DOE and DOE contractors from
Office of Scientific and Technical Information
PO Box 62
Oak Ridge, TN 37831

Prices available from (615) 576-8401, FTS 626-8401

Available to the public from
National Technical Information Service
US Department of Commerce
5285 Port Royal Rd
Springfield, VA 22161

NTIS price codes
Printed copy: A03
Microfiche copy: A01

---

SAND--89-0917

DE90 002633

SAND89–0917
Unlimited Release
Printed October 1989

# Shock-Wave Characterization of Energetic Booster-Rocket Propellant WAK-2 and Its Simulant UGS

L. J. Weirick
Explosive Projects and Diagnostics Division
Sandia National Laboratories
Albuquerque, NM 87185

## Abstract

A series of shock-loading experiments on an energetic propellant and its simulant was conducted on a light-gas gun. The purpose of this work was to characterize the shock sensitivity of WAK-2, which is a composite-modified, double-based, booster-rocket propellant and its simulant UGS. The initial objectives were to obtain Hugoniot data, to investigate the pressure threshold at which a reaction occurs, and to measure spall threshold at various impact velocities. The Hugoniot data obtained for the propellant fits the Hugoniot curve provided by the manufacturer of the propellant. A Hugoniot curve developed for the simulant was found to match that of the propellant. The initial density, $\rho_o$, initial bulk sound velocity, $C_o$, and constant S values for the energetic propellant WAK-2 and its simulant UGS were 1.85 g/cm$^3$, 2.2 mm/$\mu$s and 2.66, respectively. The ignition threshold pressure of the WAK-2 was found to be in the range of 3 kbar. A violent reaction was observed for a sample impacted at a pressure of 22 kbar. In spall tests, impact pressures in the range of 1.1 to 3.1 kbar were applied to the propellant/simulant. The propellant exhibited spall strengths ~0.33 kbar, with its simulant being somewhat weaker, ~0.22 kbar. Scanning electron microscopy and electron microprobe analysis were used to characterize the microstructures of the materials and to determine the details of the spall events.

# Acknowledgments

The author gratefully acknowledges the contributions of the following people, without whose assistance this program would not have been possible: Al Menegat, K-Tech Corp., who built targets and projectiles and operated the gas gun; Doug Dugan, 2514, who contributed much-needed technical direction to the experiments; Paul Hlava, 1822, who performed the electron microprobe analysis; Al McDonald, 8242, who instituted the program need and provided program direction and liaison; M. R. Birnbaum, 8242, who provided funding support; L. L. Bonzon, 2514, who gave managerial support, direction, and encouragement; and B. L Kistler, 8242, who improved this paper considerably by his thorough review.

# Contents

Introduction ..... 7
Experimental Procedure ..... 9
Materials ..... 9
Gas Gun ..... 15
VISAR ..... 17
Projectiles/Targets ..... 18
Results ..... 19
Hugoniot Curves ..... 19
Reaction Thresholds ..... 22
Spall Strength ..... 22
Discussion ..... 29
Hugoniot Measurements ..... 29
Reaction Threshold Measurements ..... 29
Spall Strength Measurements ..... 30
Summary ..... 31
References ..... 32

## Figures

1 Electron microprobe micrographs and elemental distribution mapping of UGS ..... 11
2 Electron microprobe micrographs and elemental distribution mapping of WAK-2 ..... 13
3 Schematic of the SNL Division 2510 gas gun system ..... 15
4 Wrap-around and dual-diaphragm gun breeches for the SNL Division 2510 gas gun ..... 16
5 Schematic of target chamber/catch tank assembly for the SNL Division 2510 gas gun ..... 16
6 Schematic of VISAR system ..... 17
7 Schematic of a Push-Pull VISAR ..... 17
8 Photograph of projectile/target assemblies for Hugoniot shots ..... 18
9 Schematic of projectile/target assemblies for spall shots ..... 19
10 VISAR record for impact of propellant onto lithium fluoride ..... 20
11 Particle velocity versus time result from Figure 10 ..... 20
12 Particle velocity versus impact stress for WAK-2 propellant and UGS simulant ..... 21
13 Particle velocity versus time records for UGS impacting quartz at various pressures ..... 23
14 Particle velocity versus time records for WAK-2 impacting lithium fluoride at various pressures ..... 23
15 Particle velocity versus time record for PMMA impacting UGS at 1.1 kbar ..... 24
16 Photograph of UGS samples after spall shots ..... 25
17 Scanning electron micrograph of UGS spall surface ..... 26
18 Particle velocity versus time record for PMMA impacting WAK-2 at 1.3 kbar ..... 27
19 Photograph of WAK-2 samples after spall shots ..... 28

## Tables

1 Properties of VRA propellant ..... 8
2 Experimental data for VRA propellant ..... 8
3 Composite formulations and mechanical properties ..... 10
4 Hugoniot results for WAK-2 propellant ..... 21
5 Hugoniot results for UGS simulant ..... 21
6 Spall results for UGS simulant ..... 25
7 Spall results for WAK-2 propellant ..... 28
8 Detonation results for VXV propellant ..... 29
9 Tensile and spall strengths of selected materials ..... 31

# Shock-Wave Characterization of Energetic Booster-Rocket Propellant WAK-2 and Its Simulant UGS

## Introduction

This investigation was done to aid in the studies of the vulnerability and lethality of solid propellant booster stages. A previous report summarized the shock characterization of a composite propellant based upon ammonium perchlorate and aluminum and its simulant.[1] This report concerns an energetic, solid propellant used in US missile boosters and the simulant for that material. The propellant of interest is WAK-2, a composite-modified, double-based propellant containing HMX high-explosive oxidizer and aluminum fuel. The simulant for this propellant, UGS, uses sodium sulfate as the inert-filler replacement for the energetic materials. A better shock characterization of the inert simulant will allow its use in testing wherever possible.

The sensitivity and power of energetic propellants have been studied since their inception. In the 1970s Lawrence Livermore National Laboratory (LLNL) performed a major experiment to determine the optimum compositions of double-based propellants and high-explosive mixes for various applications.[2] This work, together with investigations by SRI International and others, was summarized in a report from the High Energy Propellant Safety (HEPS) Committee.[3] More recently a study was done at LLNL on the detonability of energetic propellants of the composite-modified, double-base type.[4] These propellants had compositions of 40% to 50% HMX explosive (a solid oxidizer), 19% aluminum (a solid fuel), 25% energetic mix of nitrocellulose-base binder and nitroglycerine-base plasticizer (the double-base propellant), and a variety of hardeners and stabilizers.

The primary thrust of this study was to investigate delayed detonation, termed "XDT," from impacts too low in amplitude to cause direct shock initiation, termed "SDT." Parameters investigated included propellant composition, sample size, protrusions and holes, nonaxisymmetric impact, and impactor impedance. They also examined the pressure-versus-time histories of shock-loaded propellant under conditions of one-dimensional flow. LLNL found a rough trend relating XDT threshold and SDT threshold, with SDT being about twice XDT. However, many explosives and propellants comparable in shock sensitivity did not undergo XDT. They explained that the difference in behavior was most likely related to a combination of mechanical properties and binder chemistry and reported that the propellant with the highest HMX content (~50 %) and the highest binder combustion energy had an XDT of 6.2 kbar and an SDT of 13.2 kbar. Propellants with less HMX and lower binder combustion energies had respectively higher XDT and SDT values. The propellant with the lowest HMX content (~40%) and lowest binder combustion energy that they tested had an XDT of 11 kbar and an SDT of 24 kbar. This study also found that the theshold velocity for XDT reactions increases as the sample size is made smaller.

SRI International performed dynamic fracture experiments on VRA propellant, a composite-modified, double-based propellant containing both HMX oxidizer and aluminum fuel of formulation similar to WAK-2.[5] The objective of their research was to develop a fracture and fragmentation model for VRA propellant, based on the fracture kinetics of the propellant. The properties of VRA propellant are given in Table 1. An important point to notice is that the failure strength of VRA measured in a high-strain-rate (dynamic) mode is a factor of 15 greater than the failure strength measured in a low-strain-rate (static) mode. Results of SRI's plate-impact experiments on the propellant are summarized in Table 2. No damage was observed for impact stresses up to 1.4 kbar. At an impact stress of 1.58 kbar, the recovered specimen was fragmented, and at 6.3 kbar, the propellant burned. By sectioning the sample impacted at 3.5 kbar, they also found that the propellant fractured by cracking and debonding of the HMX grains, followed by propagation of intergranular cracks in the matrix material.

## Table 1. Properties of VRA propellant*

| | |
|---|---|
| Density | 1.85 g/cm$^3$ |
| Longitudinal sound velocity | 2.0 mm/ms |
| Static tension failure strength | 75 psi (0.0052 kbar) |
| Hopkinson bar failure strength | 1000-1900 psi (0.07-0.13 kbar) |

*Ref. 5.

## Table 2. Experimental data for VRA propellant*

| Shot No. | Impact Velocity (mm/μs) | Specimen Thickness† (mm) | Peak Stress‡ (kbar) | Duration of Tensile Pulse (μs) | Damage |
|---|---|---|---|---|---|
| 1419 | 0.024 | 5.97 | 0.43 | 3.60 | None |
| 1420 | 0.044 | 6.16 | 0.80 | 3.79 | None |
| 1421 | 0.310 | 6.17 | 6.30 | 3.80 | Burned |
| 1422 | 0.184 | 6.05 | 3.50 | 3.68 | Fragmented |
| 1431 | 0.110 | 6.25 | 2.08 | 3.95 | Complete spall |
| 1432 | 0.075 | 6.26 | 1.40 | 3.89 | None |
| 1433 | 0.088 | 6.31 | 1.63 | 3.94 | Internal spall |
| 1434 | 0.084 | 6.30 | 1.58 | 3.93 | Internal spall |

*Ref. 5.
†Projectile head thickness was 3.43 mm.
‡Peak tension assumed the same as peak stress.

As pertains to this study here, the shock Hugoniot of a material is determined when the relationship between the shock and particle velocities is known. This relationship can be experimentally determined from planar, gun-impact experiments and can generally be approximated by a linear fit,

$$U_s = C_o + SU_p \ , \qquad (1)$$

where

$U_s$ is the shock velocity
$C_o$ is the initial bulk sound velocity
S is a dimensionless, empirical parameter
$U_p$ is the particle velocity.

In addition to Hugoniot data, this study measured spall strengths of the materials in question. The process of spallation has been studied in a number of laboratories to obtain the criteria for dynamic fracture at high stress rate. Tension is induced within a sample by allowing a stress wave to reflect as a rarefaction from a free surface. The tension increases by interaction of the rarefaction wave with the primary wave until a critical value is reached and fracture occurs. The fact that the free-surface velocity stops dropping and then rises (spall rebound or "pullback") is caused by the generation of compressive waves at the spall plane that increase the pressure. The clearly defined onset of fracture at a specific value of pullback suggests a characteristic material strength that corresponds to a damage threshold tension. This material property is referred to as the incipient fracture strength or spall strength, $\sigma$. The value of $\sigma$ may be approximately related to the observed pullback by considering the interaction of the reflected wave with the primary wave, assuming a perfect reflection at the free surface.[6] The resultant expression is:

$$\sigma = 1/2 \ C_o \ \rho_o \ \Delta\mu \ , \qquad (2)$$

where

$C_o$ is the initial bulk sound velocity
$\rho_o$ is the material density
$\Delta\mu$ is the measured pullback.

The incipient fracture is understood in material terms as the macroscopic yield stress necessary for the growth of internal voids into a free surface or spall plane. One method of observing the details of the complete fracture history has been free-surface velocity measurements using a laser interferometer.[7,8]

The objectives of this study are to obtain Hugoniot data, to investigate the pressure threshold at which a reaction occurs, and to measure spall damage at various impact velocities.

# Experimental Procedure

## Materials

The materials of interest in this study are a solid rocket booster propellant designated WAK-2 and its simulant designated UGS. They were manufactured by Morton-Thiokol, Wasatch Operations, Brigham City, Utah. The materials of which the WAK-2 and UGS were composed are given in Table 3 along with the formulation for UGS.[9] The details of the formulation for WAK-2 are classified. Microstructure characterization of UGS and WAK-2 was done by using the electron microprobe. Figure 1 shows a scanning electron micrograph (SEM) and a back scattered electron (BSE) micrograph of a cut surface of UGS along with accompanying elemental distribution maps (EDM). (An EDM is an x-y map of the chosen element exposed by the x-ray emitted when an electron was knocked from the element's orbit by a bombarding electron from the primary electron beam.) First, the material has no significant porosity, it being a cast material rather than compressed granules. Second, the large crystals are sodium sulfate, which is used as the inert, filler material in the simulant (indicated by the Na, S, and O maps). Third, the small and diffused, spherically shaped particles are metallic aluminum, which is used as one of the fuels (indicated by the Al map). Fourth, the matrix binding these constituents together is a mix of hexane diol adipate phythalate (HDAP) and the nitrocellulose-base portion of the double-base propellant (DBP). These materials are represented by the C map. The simulant is considered to have a "medium coarseness" of microstructure because of the large sodium sulfate crystals.

**Table 3. Composite formulations and mechanical properties**

| | WAK-2 | UGS (wt %) | |
|---|---|---|---|
| COMPOSITION | | | |
| Fuel | Double-base propellant | DBP | 19.7 |
| | Aluminum | Al | 5.0 |
| Oxidizer | HMX | HMX | 0.0 |
| | Ammonium perchlorate | AP | 0.0 |
| Inerts | | $NaSO_4$ | 65.3 |
| Polymers | | HDAP | 9.0 |
| Curatives | | N100 | 1.0 |
| Processing aid | | HDI | 0.04 |
| MECHANICAL PROPERTIES | | | |
| Density ($g/cm^3$) | 1.85 | | 1.85 |
| Tensile strength (psi/kbar) | 100.0/0.007 | | 158.0/0.011 |
| Maximum elong. (%) | 250.0 | | 50.0 |
| Tensile modulus (psi) | 450.0 | | 490.0 |

The propellant formulation is based on a composite-modified (HMX, aluminum, and ammonium perchlorate additions), double-base mix (nitrocellulose and nitroglycerin). Figure 2 shows electron microprobe micrographs and EDMs of a cut surface of WAK-2. This material does not exhibit any significant porosity, being a cast material rather than compressed granules. The size, shape, and distribution of the aluminum particles are readily apparent in the EDM for Al. Similarly, the size and distribution of the ammonium perchlorate (AP) particles are indicated by the Cl map. The carbon and oxygen EDMs show the homogeneity of the organic mix of the nitroglycerine-base portion of the DBP and HMX oxidizers as bonded by the nitrocellulose. The propellant microstructure can be described as having a medium coarseness.

The "static" mechanical properties of both materials are also given in Table 3. The tensile strengths of these materials are very low: 0.011 and 0.007 kbar, or 158 and 100 psi, for the simulant and propellant, respectively. The maximum elongation of the simulant is moderate, 50%, and that of the propellant is very high, 250%. The densities of these materials of 1.85 $g/cm^3$ are typical of solid rocket booster propellants.

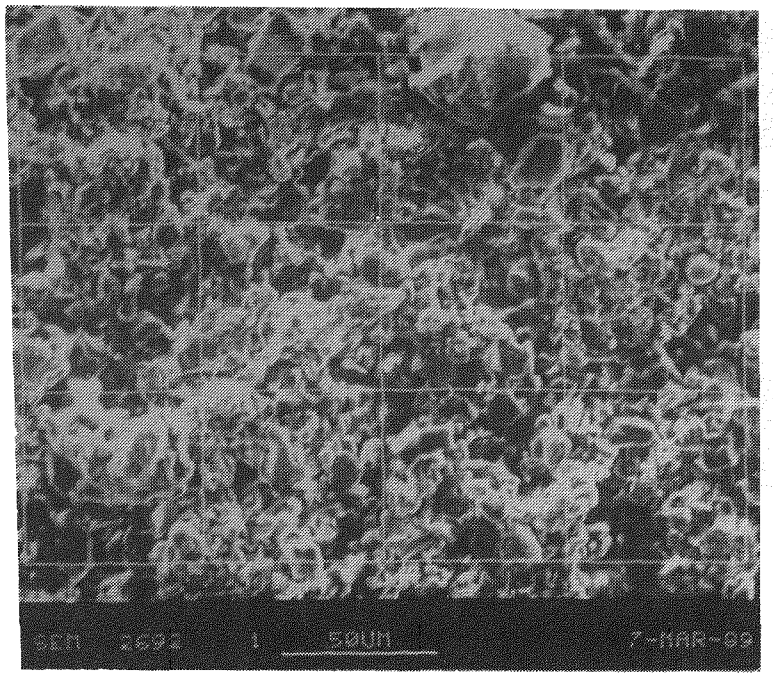

SCANNING ELECTRON

MICROGRAPH

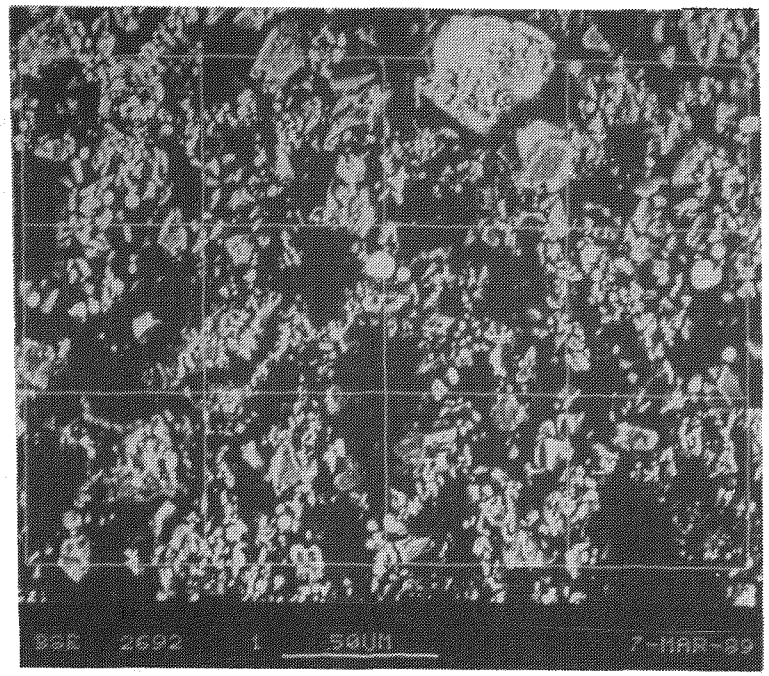

BACK-SCATTERED ELECTRON

MICROGRAPH

UGS SIMULANT

**Figure 1.** Electron microprobe micrographs and elemental distribution mapping of UGS (continued)

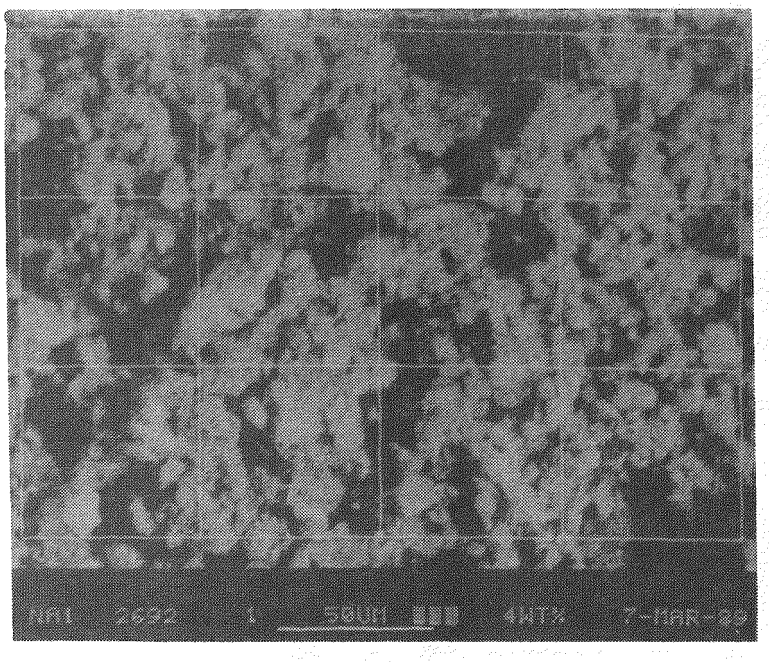

SODIUM

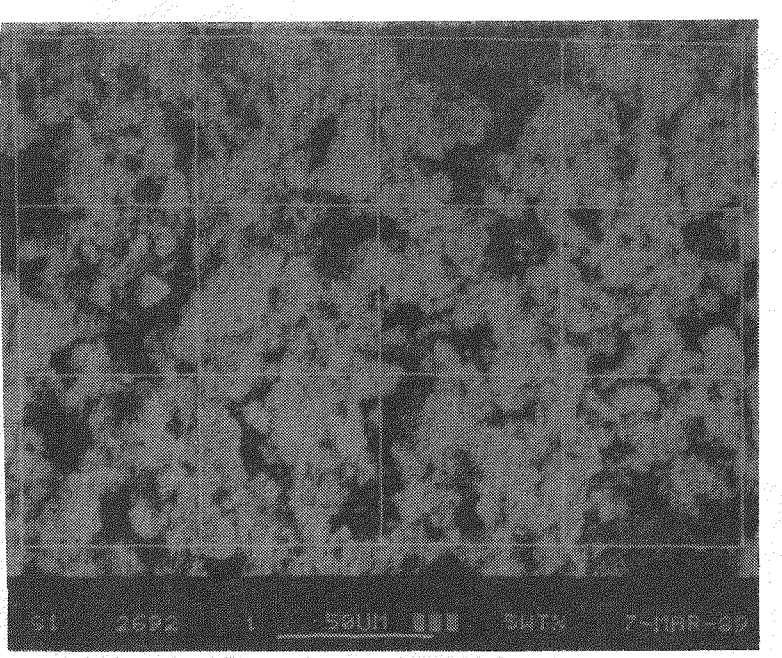

SULFUR

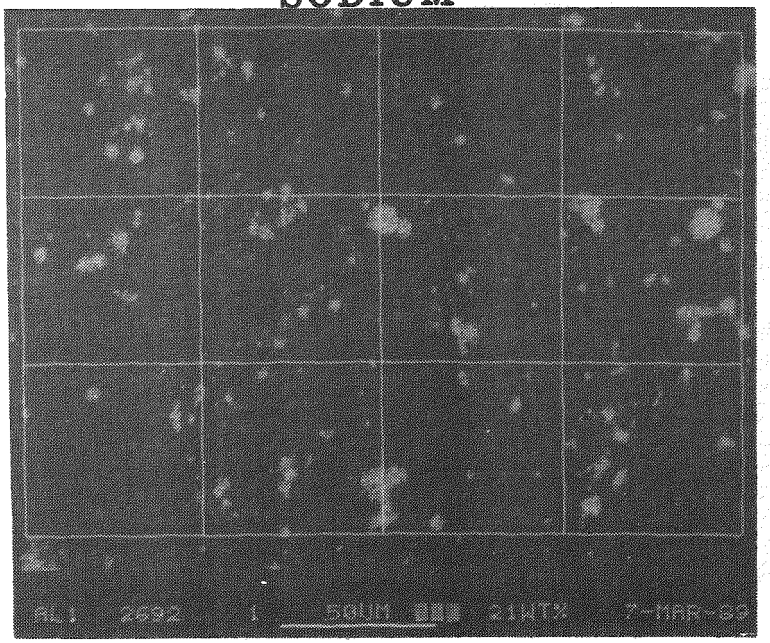

ALUMINUM

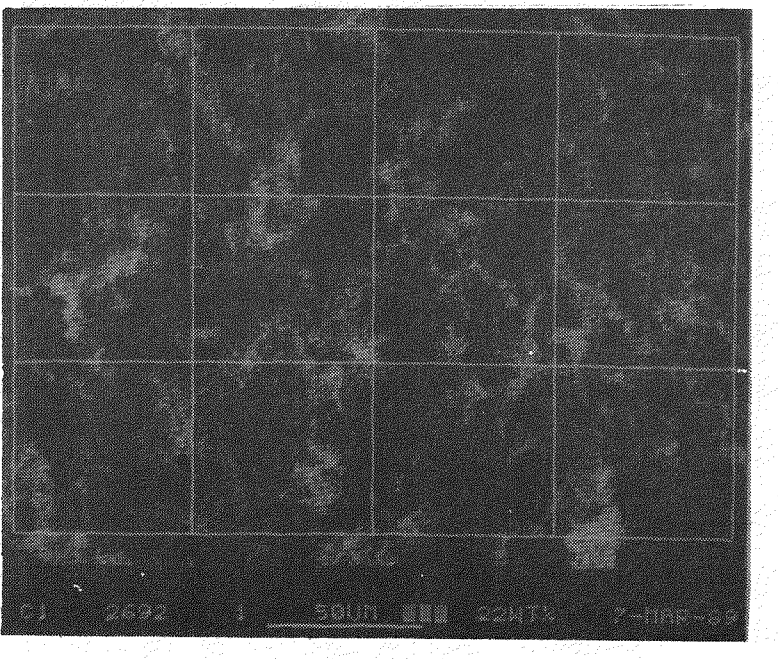

CARBON

**Figure 1.** (concluded)

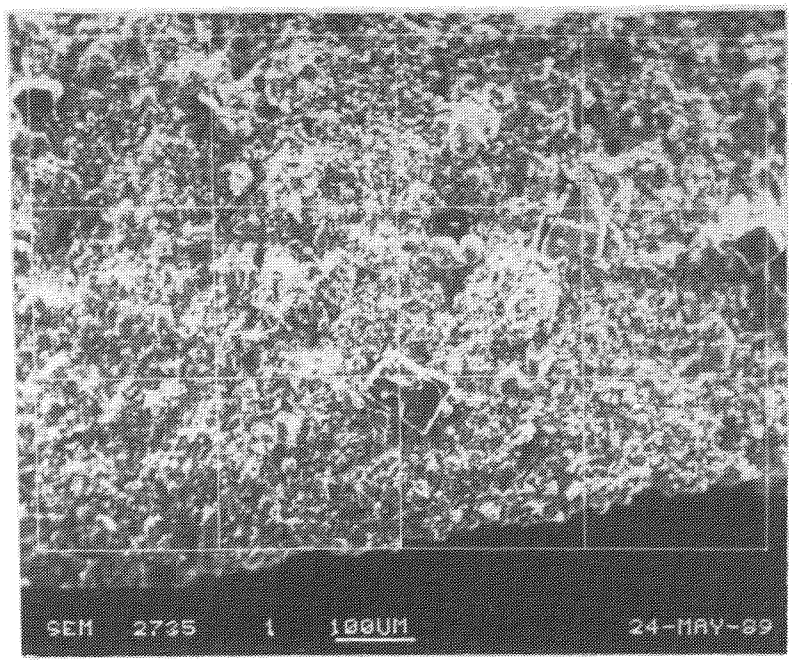


SCANNING ELECTRON

MICROGRAPH

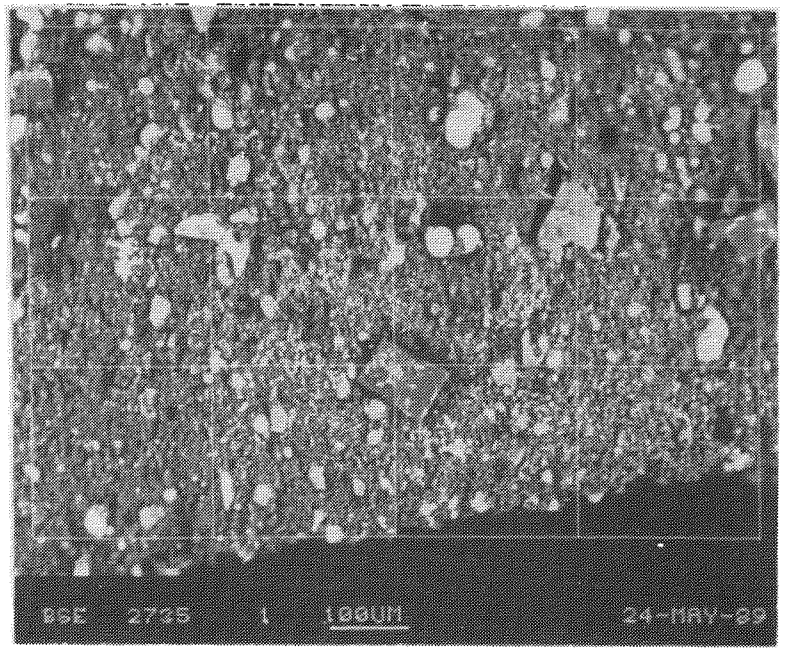


BACK-SCATTERED ELECTRON

MICROGRAPH

**Figure 2.** Electron microprobe micrographs and elemental distribution mapping of WAK-2 (continued)

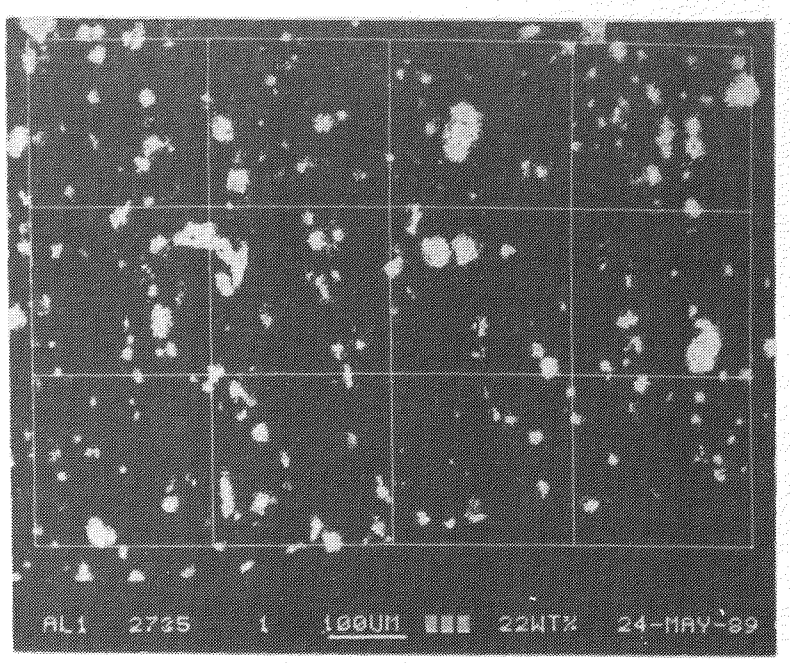


ALUMINUM

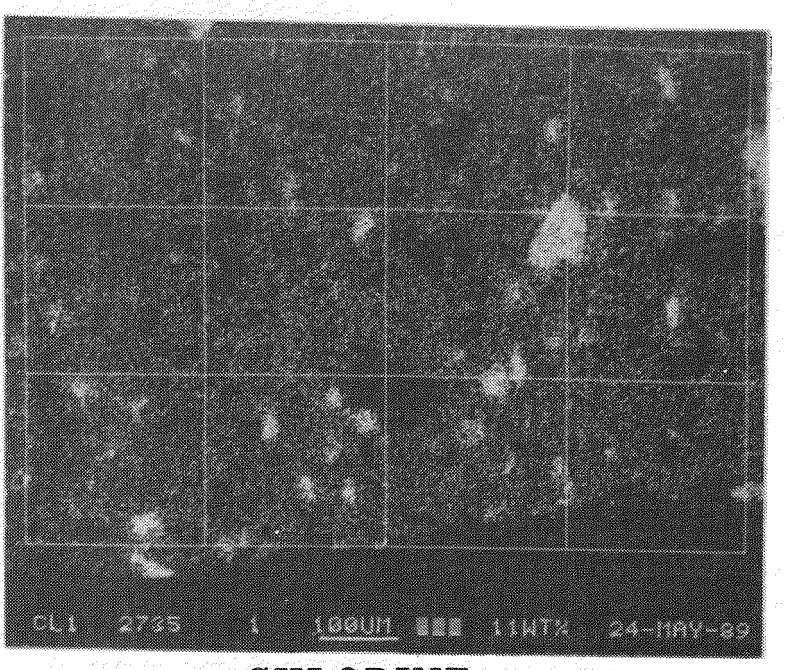


CHLORINE

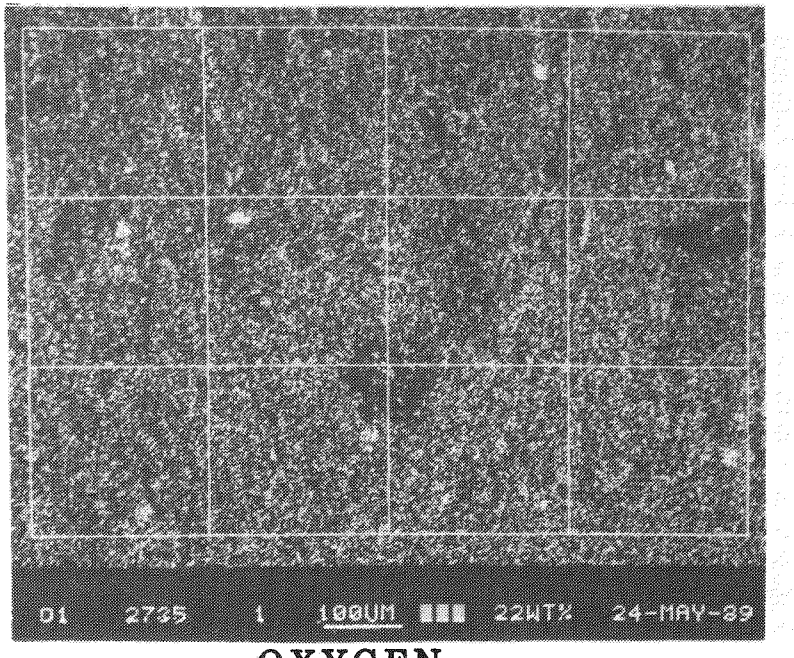


OXYGEN

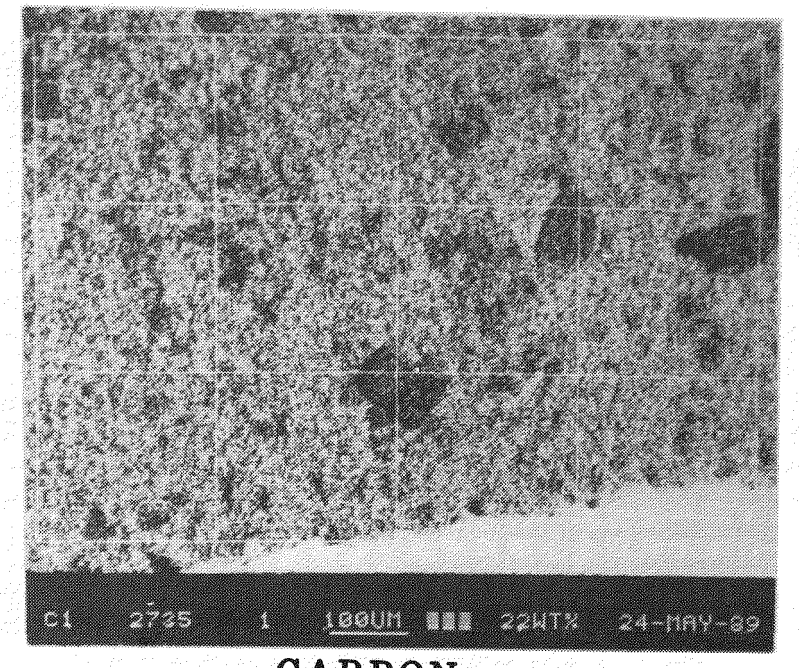


CARBON

**Figure 2.** (concluded)

## Gas Gun

A gas gun was used for most of the experiments in this study. A schematic of the gun system is shown in Figure 3.[10] The gun barrel is 9 m long, with an inside diameter of 63.4 mm (~2-1/2 in.). The breech is of a quick-acting, quick-change design, with two inserts: one termed a "wrap-around" (Figure 4) for low-velocity shots (below 0.5 km/s) and a second called a "dual-diaphragm" (also shown in Figure 4) for higher-velocity shots. The gas used to pressurize the breech is nitrogen for low-velocity shots and helium for higher-velocity shots. When helium is used at a maximum pressure of 42 MPa (6 ksi), a projectile velocity of 1.5 km/s may be attained for projectiles with weights below 0.2 kg.

The target mount consists of a target platform attached to three remotely driven differential screws that allow the operator to align the target to the chosen angle and distance from the barrel end (Figure 5). Theoretically, the impact planarity obtainable is 0.03 mrad. Experimentally, the planarity was below 0.5 mrad. The target chamber has 1.6-cm-thick steel walls that allow a 100-g sample of explosive to be contained upon detonating. A catch tank attached to the end of the target chamber is filled with high-strength parachute fabric, which absorbs the momentum of the projectile and target fragments. A 25-cm-thick steel plate at the end of the catch tank ensures containment of a heavy projectile. A thin Mylar diaphragm is used between the target chamber and catch tank to isolate the target chamber so that it can be evacuated along with the barrel to <15-$\mu$m pressure before a shot.

The pressurization and firing sequence is controlled by a Hewlett Packard 86 computer. The computer program leads the operator through the setup operations, monitors the gun's interlocks, and opens and closes the appropriate valves to initiate pressurization and firing.

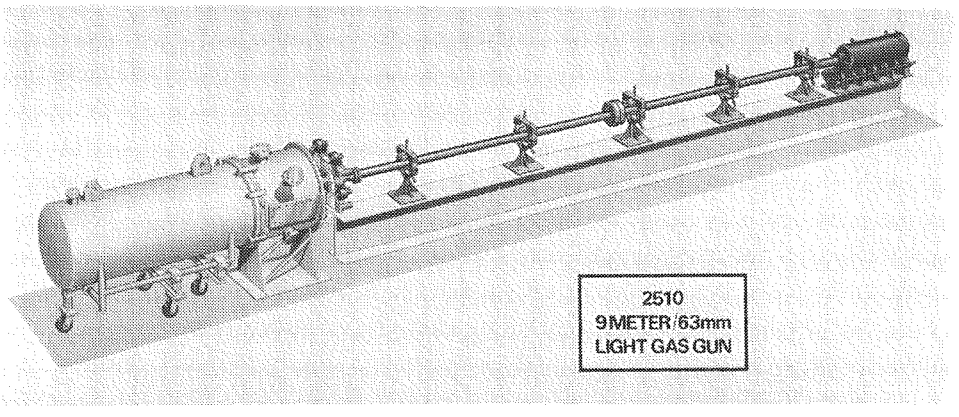


**Figure 3.** Schematic of the SNL Division 2510 gas gun system

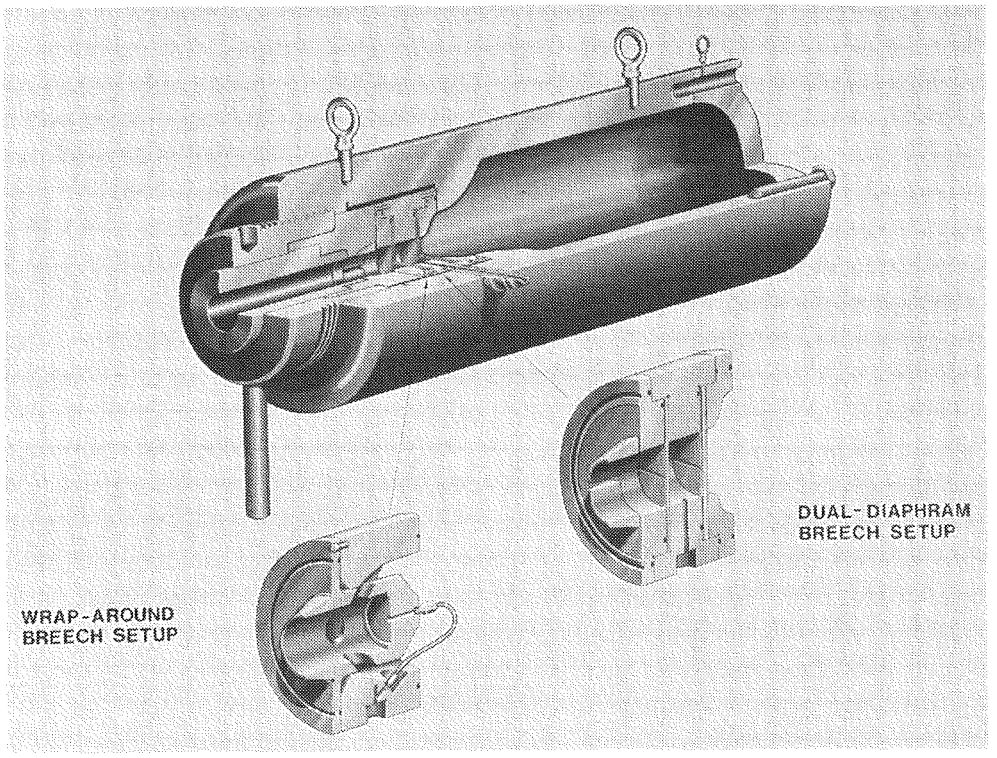


**Figure 4.** Wrap-around and dual-diaphragm gun breeches for the SNL Division 2510 gas gun

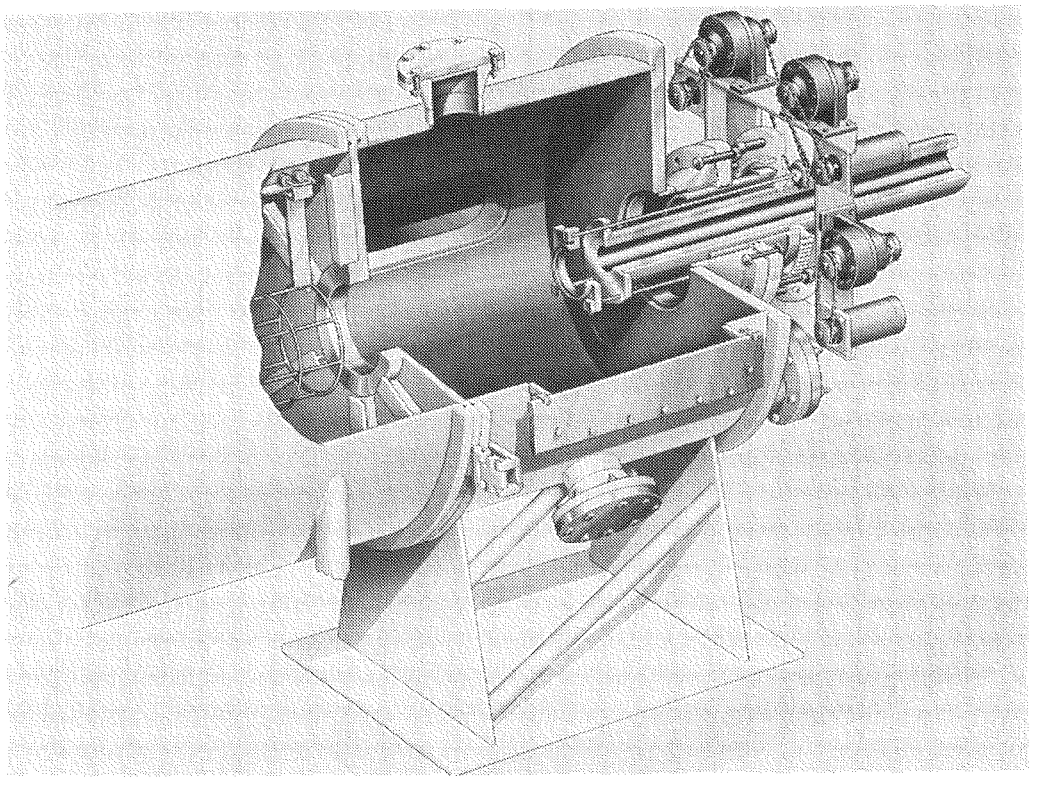

**Figure 5.** Schematic of target chamber/catch tank assembly for the SNL Division 2510 gas gun

## VISAR

The technique used for measurement of shock phenomena was a VISAR (Velocity Interferometer System for Any Reflector).[11] This modern technique uses coherent, monochromatic light from a laser source to measure the motion of a diffuse reflective surface. The Doppler shift in the reflected light is detected in a modified Michelson interferometer. The inherent sensitivity, resolution, and frequency response of such a system are essentially limited only by the bandwidth of the optical detectors and recording equipment.

The features of a conventional VISAR are shown in Figure 6. A diffused beam containing the target Doppler information is returned to the VISAR table, passing through a telescope to reduce the beam diameter. After passing through a beamsplitter, half of the signal is sent through a reference leg and half through a delay leg whose medium is air and quartz. This beam is delayed because of the difference in the index of refraction of the quartz versus air. The beams are reflected and recombined at the main beamsplitter, where interference occurs. An interference fringe is produced in the recombined beam by a change in the target velocity. A polarizing beamsplitting cube splits the beam into two quadrature components: P, the transmitted beam, and S, the reflected beam. The target velocity information is contained in the fringe-time history of each of the S- and P-polarized light beams. These beams are monitored by photomultiplier tubes. The P-polarized light is labeled Data 1, and the S-polarized light is labeled Data 2 in Figure 6.

In some shock-wave experiments, such as those involving energetic materials, self-light from the target device can result in a large, unwanted optical signal to the optical detectors. A "Push-Pull" VISAR method (Figure 7; developed by Hemsing[12]) results in effective cancellation of self-light as a common-mode signal. This design, which uses the wasted light beam from the main beamsplitter, also improves the signal-to-noise ratio by doubling the signal amplitude. Furthermore, the method results in simplified data acquisition and reduction. The Push-Pull VISAR technique was used for Hugoniot and reaction threshold measurements.

An important variation on the Push-Pull VISAR is a system with an extended (e.g., 166-cm-long) air-delay leg in place of the quartz-delay leg. This replacement allows the accurate measurement of particle velocity in a very-low-velocity regime, i.e., below 0.1 km/s. The air-delay leg VISAR was used for spall strength measurements.

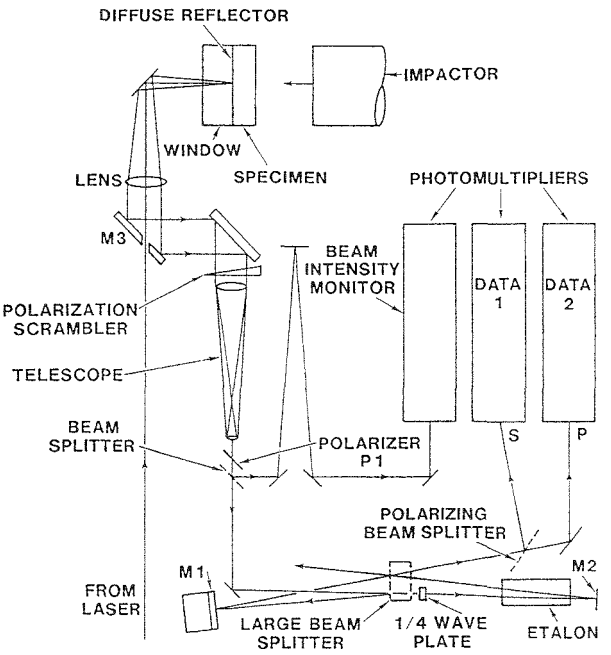


**Figure 6.** Schematic of VISAR system

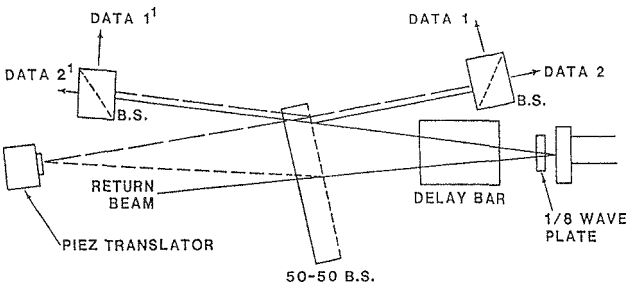


**Figure 7.** Schematic of Push-Pull VISAR

# Projectiles/Targets

## Hugoniot/Reaction Threshold Setup

Figure 8 is a photograph of the projectile/target assemblies used for obtaining Hugoniot and reaction threshold data. A 5-cm-dia by 1.2-cm-thick disc (50 g) of propellant/simulant is epoxied to the front end of a lightweight (200 g) nylon/foam projectile. By using lightweight projectiles and pressurizing the breech with helium, projectile velocities near 1.5 km/s can be attained. The targets for the propellant shots consisted of 6.2-cm-dia by 2.54-cm-thick discs of lithium fluoride (LiF). The targets for the simulant shots consisted of 6.2-cm-dia by 1.27-cm-thick discs of quartz (Dynasil 1000). LiF was used for the propellant shots because it has a higher pressure range of application. The LiF discs were also thicker than the quartz discs, which produced in a longer recording time of the VISAR signal before geometrical interference. A layer of aluminum was evaporated onto the front of the target material that was used as the reflector for the laser beam. The laser beam comes in from the back of the target and is reflected off the back surface of the aluminum mirror. A 1.0-mm-thick lithium fluoride or quartz plate was epoxied on the front of the target as a buffer. The buffer plate smooths the spatial nonuniformities in the wavefront generated at the impact interface and generates some initial fringes that simplify the VISAR data reduction.

## Spall Setup

A schematic of the projectile/target setup for obtaining spall strength data is shown in Figure 9. A 5-cm-dia by 0.75-cm-thick disc of propellant/simulant is epoxied to an aluminum ring holder on the target mount. A 0.01-mm-thick piece of aluminum foil is epoxied with urethane cement to the back side of the propellant/simulant disc to function as a reflecting free-surface mirror for the laser beam. The projectiles are designed for maximum weight (3.5 kg) by using aluminum cylindrical shells containing a lead-shot/epoxy mix. A 0.32-cm-thick PMMA disc (low-impedance impactor) is attached to a 6-mm-long, aluminum standoff ring at the front of the projectile. By using heavy projectiles and pressurizing the breech with nitrogen, the best control for very low projectile velocities (0.01 km/s) can be attained.

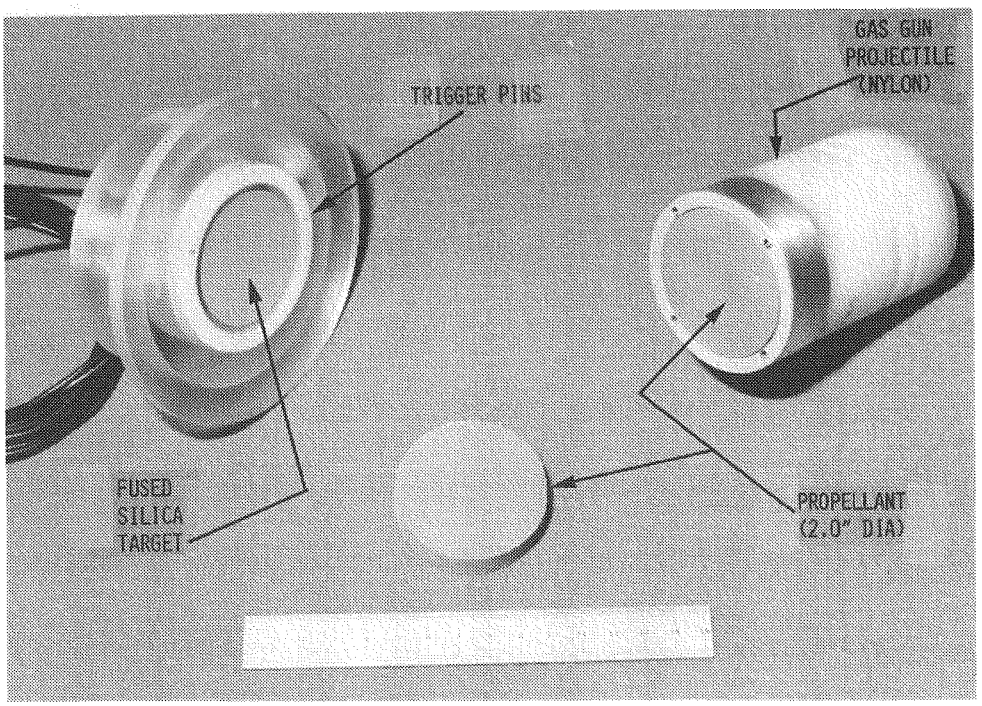


**Figure 8.** Photograph of projectile/target assemblies for Hugoniot shots

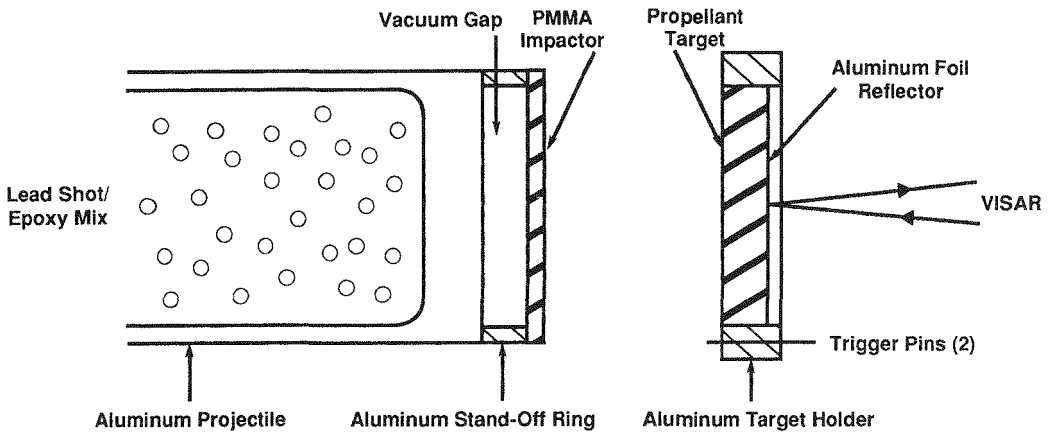


**Figure 9.** Schematic of projectile/target assemblies for spall shots

# Results

## Hugoniot Curves

### WAK-2 Propellant

Figure 10 shows the VISAR record for the impact of a propellant disc onto a lithium fluoride target at an impact pressure of 22 kbar (0.53 mm/ms). The VISAR fringes record the velocity jump at impact. The fringe information is reduced by using the relationship between the instantaneous interference fringe count and the velocity of the target.[13] The fringe count from the initial fringe position as a function of time is multiplied by the velocity-per-fringe (VPF) scaling factor to obtain the particle velocity as a function of time, as shown in Figure 11.

Propellant discs were impacted at velocities ranging from 0.15 to 0.53 mm/$\mu$s (impact pressures from 5.3 to 22.0 kbar), and the resultant particle velocities were determined. These test parameters and results are summarized in Table 4. Plotting the particle velocities versus the stress (impact pressure) gives the Hugoniot curve for this propellant (Figure 12). The solid curve is the Hugoniot calculated from the Hugoniot parameters provided by the manufacturer of the propellant, Morton-Thiokol. The Hugoniot relationship of a material is expressed as the relationship between the shock and particle velocities and can be experimentally determined from the Hugoniot data and Eq (1). The initial density, $\rho_o$, initial bulk sound velocity, $C_o$, and coefficient S values for the energetic propellant WAK-2 were found to be 1.85 g/cm$^3$, 2.2 mm/$\mu$s, and 2.66, respectively.

### UGS Simulant

Simulant discs were impacted at velocities ranging from 0.25 to 1.00 mm/$\mu$s (impact pressures from 9.1 to 43.8 kbar), and the resultant particle velocities were determined. The test parameters and results are summarized in Table 5. Plotting the particle velocities versus the stress (impact pressure) gives the Hugoniot curve for this simulant as shown in Figure 12, where it is also compared with the Hugoniot curve for WAK-2. The initial density, $\rho_o$, initial bulk sound velocity, $C_o$, and coefficient S for the simulant UGS were found to be 1.85 g/cm$^3$, 2.2 mm/$\mu$s, and 2.66, respectively, the same as those for the propellant.

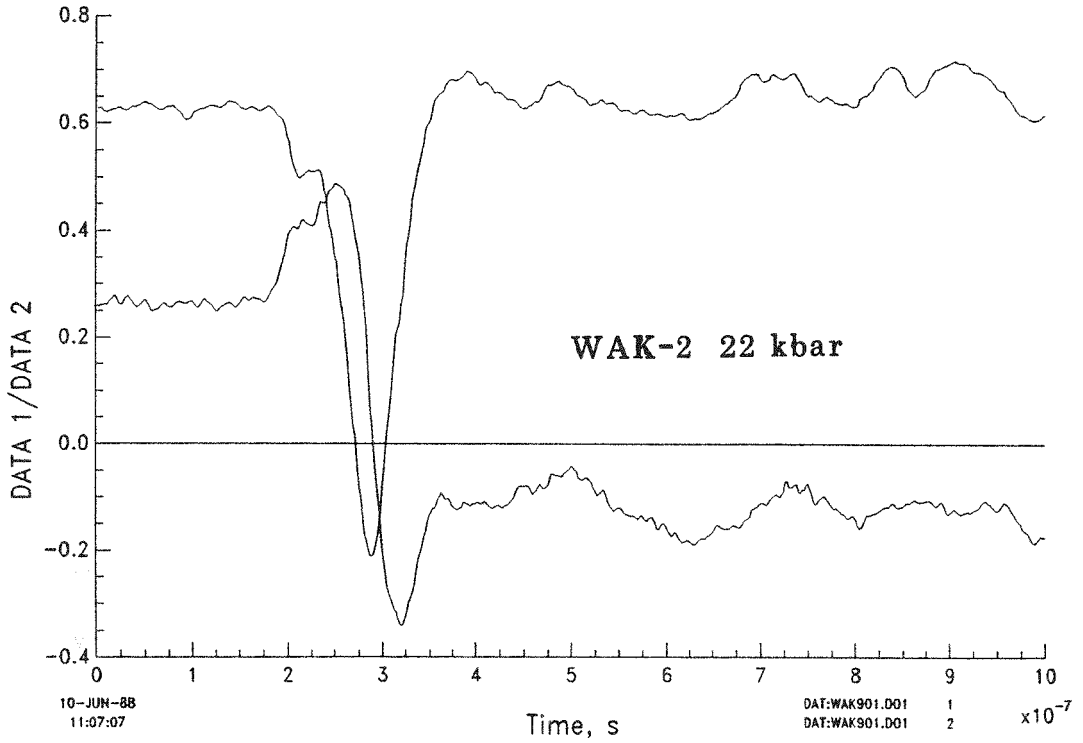


**Figure 10.** VISAR record for impact of propellant onto lithium fluoride

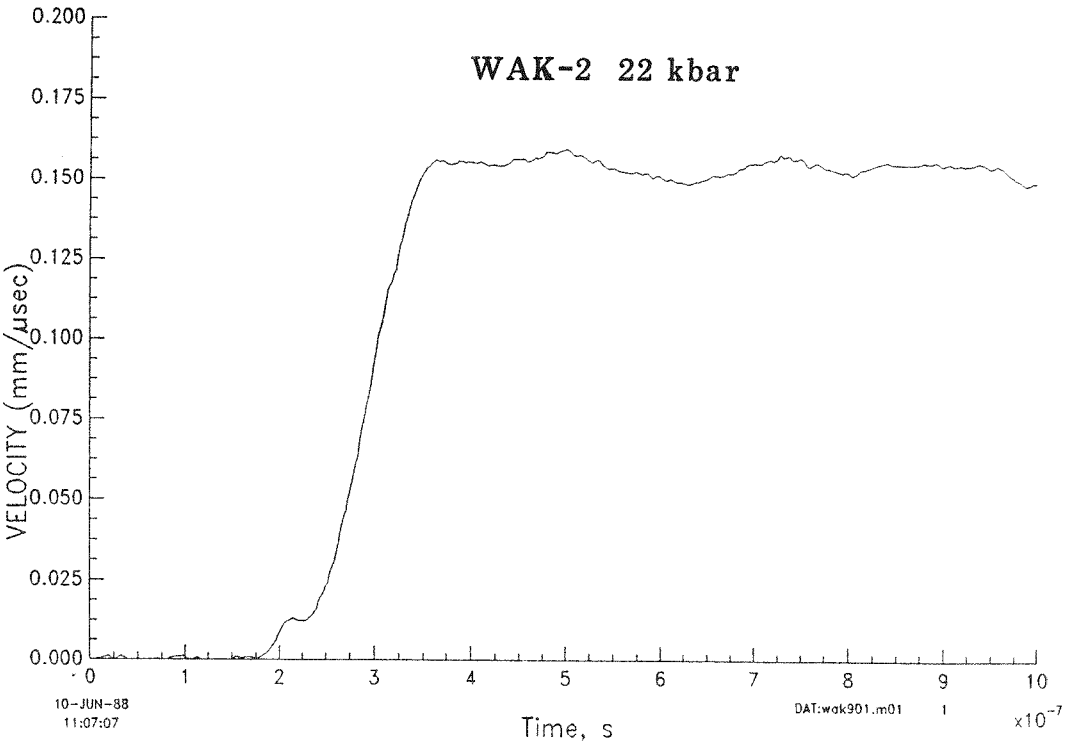


**Figure 11.** Particle velocity versus time result from Figure 10

## Table 4. Hugoniot results for WAK-2 propellant

| Projectile Velocity Measured Pins (mm/μs) | Particle Velocity Predicted Hugoniot* (mm/μs) | Particle Velocity Measured VISAR† (mm/μs) | Impact Pressure (kbar) | Comments |
|---|---|---|---|---|
| 0.15 | 0.038 | 0.037 | 5.3 | Reaction initiated |
| 0.25 | 0.066 | 0.067 | 9.1 | Mild reaction |
| 0.53 | 0.155 | 0.156 | 22.0 | Detonation? |

*WAK-2:LiF
†$\Delta v/v_0 = 0.26$

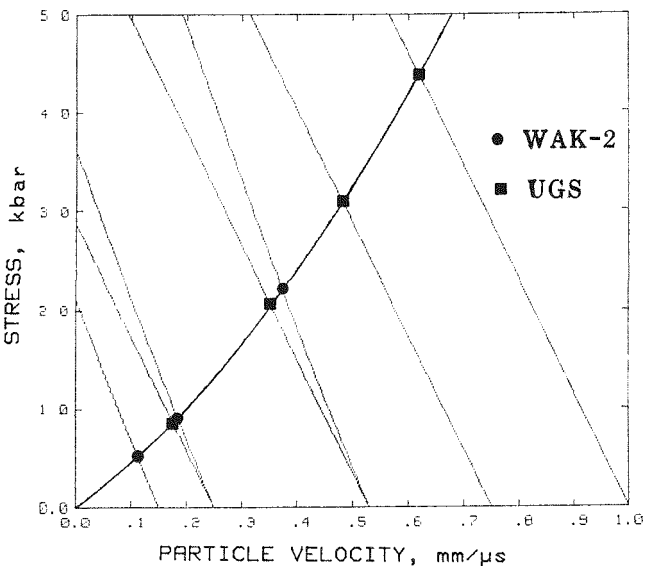


**Figure 12.** Particle velocity versus impact stress for WAK-2 propellant and UGS simulant

## Table 5. Hugoniot results for UGS simulant

| Projectile Velocity Measured Pins (mm/μs) | Particle Velocity Predicted Hugoniot* (mm/μs) | Particle Velocity Measured VISAR† (mm/μs) | Impact Pressure (kbar) |
|---|---|---|---|
| 0.25 | 0.074 | 0.073 | 9.1 |
| 0.53 | 0.177 | 0.170 | 20.4 |
| 0.75 | 0.268 | 0.270 | 30.9 |
| 1.00 | 0.381 | 0.370 | 43.8 |

*WAK-2:Fused Silica
†$\Delta v/v_0 = 0.04$

## Reaction Thresholds

### UGS Simulant

When a material that does not subsequently react, such as a simulant, is impacted, the velocity record should show a jump at impact to the equilibrium particle velocity and then remain constant with time until release waves from side walls or rear surfaces reach the observation point. Figure 13 gives the particle velocities versus time records for UGS impacting quartz at various pressures. At impact, the relative particle velocities of the quartz jumped to the equilibrium values and remained essentially constant for 2.3 $\mu$s (for impact pressures of 20.4, 30.9, and 43.8 kbar), at which time the shock wave reached the free surface of the 12.7-mm-thick window. The resulting reflected rarefaction wave began distorting the window, and the VISAR signal deteriorated and then was lost. The record for the impact of UGS at 9.1 kbar shows the jump to the equilibrium particle velocity, which then remained constant for the length of the record, 3.5 $\mu$s. The particle velocity signal remained constant for this shot because the target was 25.4 mm thick, and the signal drop-off was not expected until 4.6 $\mu$s.

In addition, Figure 13 indicates that the particle velocity records became "noisier" as the impact pressure was increased.

### WAK-2 Propellant

When a material that subsequently reacts, such as a propellant, is impacted, the velocity record should show a jump at impact to the equilibrium particle velocity, remain constant with time during an initiation period, and then increase with time as the reaction grows. The particle velocity record for lithium fluoride upon being impacted by WAK-2 at 0.53 mm/$\mu$s (22.0-kbar impact pressure) is shown in Figure 14. At impact, the particle velocity of the quartz jumped to ~0.156 mm/$\mu$s and remained essentially constant for 3.5 $\mu$s. At 3.5 $\mu$s after impact, the velocity begins to steadily increase, indicating the initiation of a reaction within the WAK-2 propellant. The velocity, and thus the reaction, steadily increased until 5 $\mu$s after impact, at which time the velocity had increased beyond the scale of the recording equipment. Posttest observation of the test hardware indicated that a violent reaction had occurred. The propellant had completely reacted and no remnant traces were recovered. The target holder and focusing mirror had disintegrated. In addition, significant smoke was observed in the target chamber, and the recovery parachute material had melted around fragments.

Figure 14 also shows the particle velocity versus time record for WAK-2 impacting lithium fluoride at 9.1-kbar impact pressure. At impact, the particle velocity of the quartz jumped to ~0.067 mm/$\mu$s and remained essentially constant for 3 $\mu$s. At this time (3 $\mu$s), the propellant began to react, and the reaction and velocity increased until the signal went off-scale. Posttest observation of the test hardware confirmed that a reaction had occurred. The target holder and associated hardware were fragmented, without remnants of propellant. However, no smoke was observed in the target chamber, and the parachute recovery material had not melted around any fragments.

Impacting WAK-2 onto lithium fluoride at an impact pressure of 5.3 kbar produced an interesting result, also shown in Figure 14. The particle velocity jumped to 0.037 mm/$\mu$s and remained constant for 3.3 $\mu$s, at which time a reaction began and the particle velocity increased, a pattern analogous to the other WAK-2 tests. However, after 3 $\mu$s of reaction time, the particle velocity stopped increasing and decreased, indicating that the reaction had ceased. Posttest observation of the test hardware gave no evidence of a reaction (the target holder and focusing mirror were intact, and the propellant was mechanically damaged but unreacted).

## Spall Strength

As mentioned previously, the static tensile strengths of WAK-2 and UGS are low, around 0.01 kbar (145 psi). Thus, spall strengths of these materials are also expected to be low since the spall strengths of most materials (plastics, metals, ceramics, explosives) are typically two to ten times greater than the static tensile strengths. To accurately measure spall strengths this low, it is necessary to impact the material with low-impedance projectiles at low velocities.

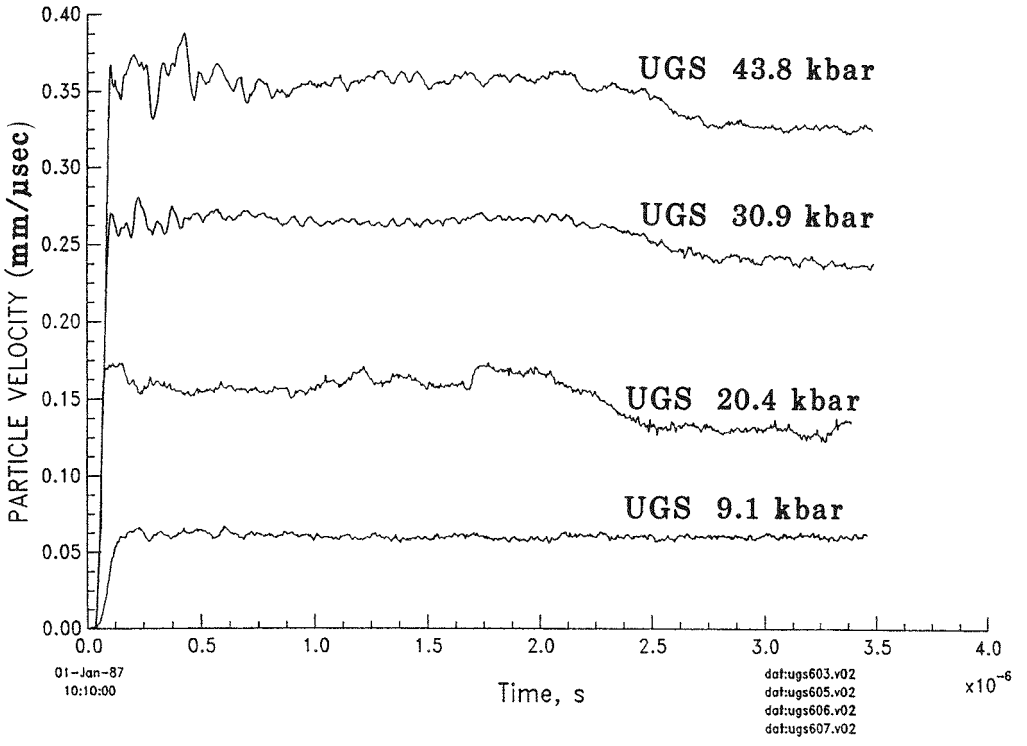


**Figure 13.** Particle velocity versus time records for UGS impacting quartz at various pressures

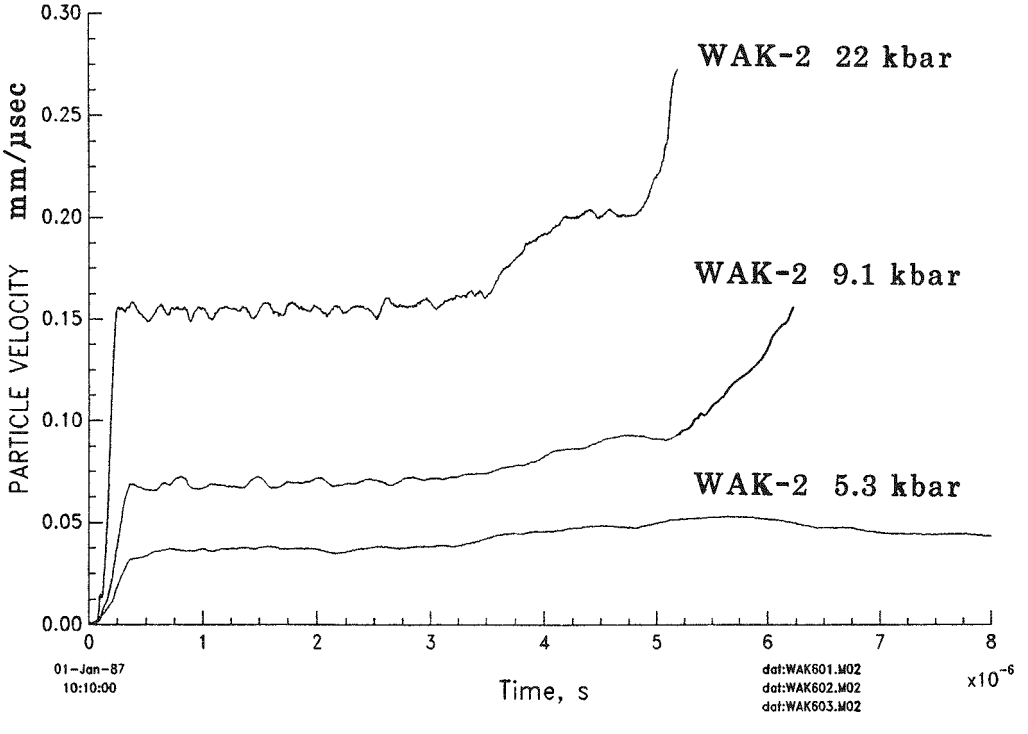


**Figure 14.** Particle velocity versus time records for WAK-2 impacting lithium fluoride at various pressures

## UGS

Spall shots were done on UGS at impact pressures from 1.1 to 3.1 kbar, with projectile velocities of 62 to 167 m/s, respectively. An example of the resultant particle velocity versus time plot for UGS impacted by PMMA is shown in Figure 15. This example is for an impact pressure of 1.1 kbar, corresponding to a projectile velocity of 62 m/s. The spall strength of UGS calculated for this shot using Eq (2) with velocity pullback of 0.011 mm/μs, density of 1.85 g/cm$^3$, and sound velocity of 2.2 mm/μs, is 0.224 kbar (3250 psi). The results for this set of spall tests on UGS are tabulated in Table 6, which also lists the particle velocities calculated from the Hugoniot data for the respective projectile velocities. Twice the values of these particle velocities should approximately equal the measured free-surface velocities.

Figure 16 shows cross sections of the UGS samples after the spall shots. The spall planes are readily visible in the samples. Figure 17 shows high magnification SEM micrographs taken at the end of the crack in the UGS sample impacted at 0.63 kbar. These micrographs show the path of the fracture plane winding around the $NaSO_4$ crystals and Al particles through the double-base propellant and HDAP. They also show the elasticity of the binder material (the gummy stringers).

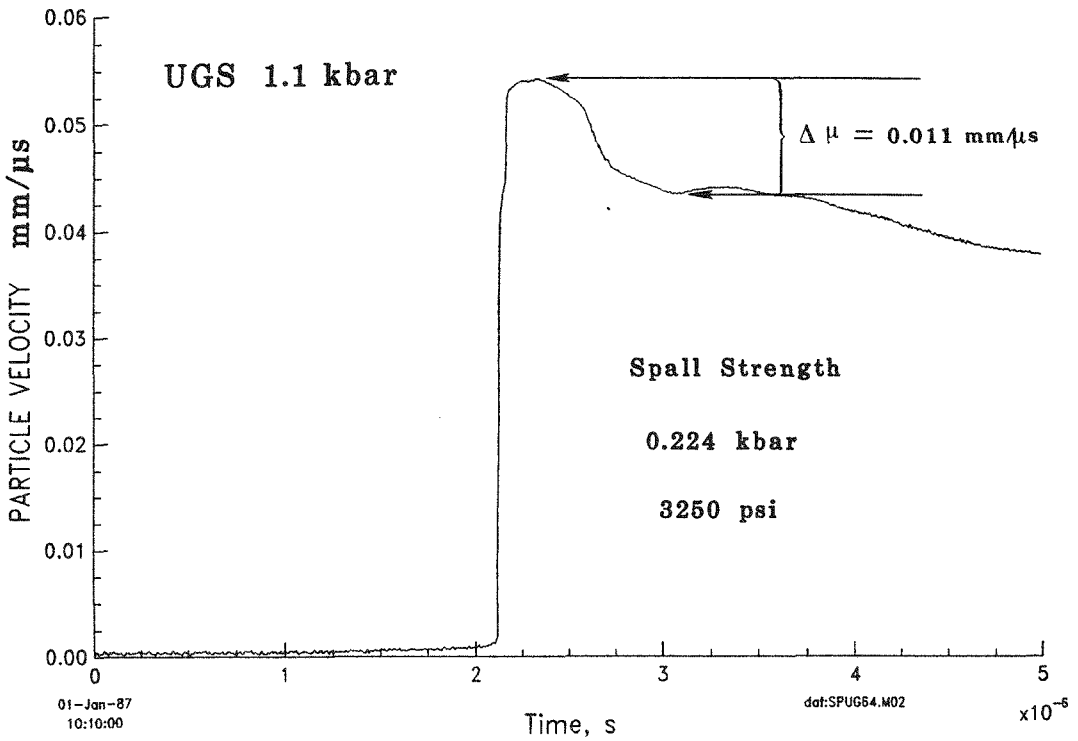


**Figure 15.** Particle velocity versus time record for PMMA impacting UGS at 1.1 kbar

## Table 6. Spall results for UGS simulant

| Projectile Velocity Measured (m/s) | Particle Velocity Calculated* (m/s) | X2 (m/s) | Free-Surface Velocity Measured (m/s) | Impact Stress Calculated | | Spall Strength Measured | |
|---|---|---|---|---|---|---|---|
| | | | | (kbar) | (ksi) | (kbar) | (ksi) |
| 62 | 26.5 | 53.0 | 54.0 | 1.11 | 16.10 | 0.224 | 3.25 |
| 132 | 56.0 | 112.0 | 110.0 | 2.42 | 35.09 | 0.214 | 3.100 |
| 167 | 70.7 | 141.4 | 142.0 | 3.10 | 44.95 | 0.305† | 4.425 |

*WAK-2:PMMA
†Best estimate

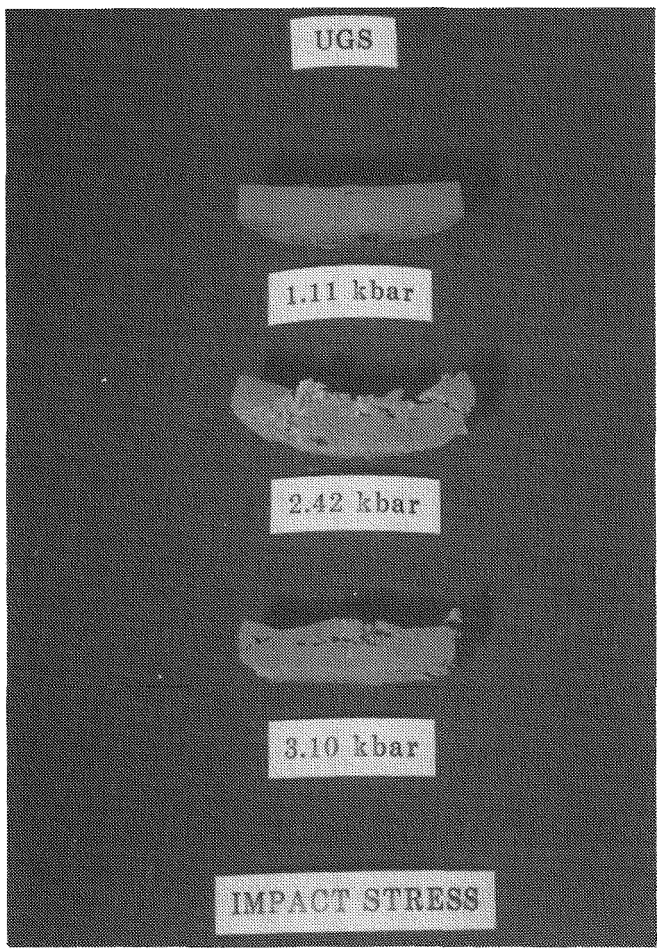


**Figure 16.** Photograph of UGS samples after spall shots

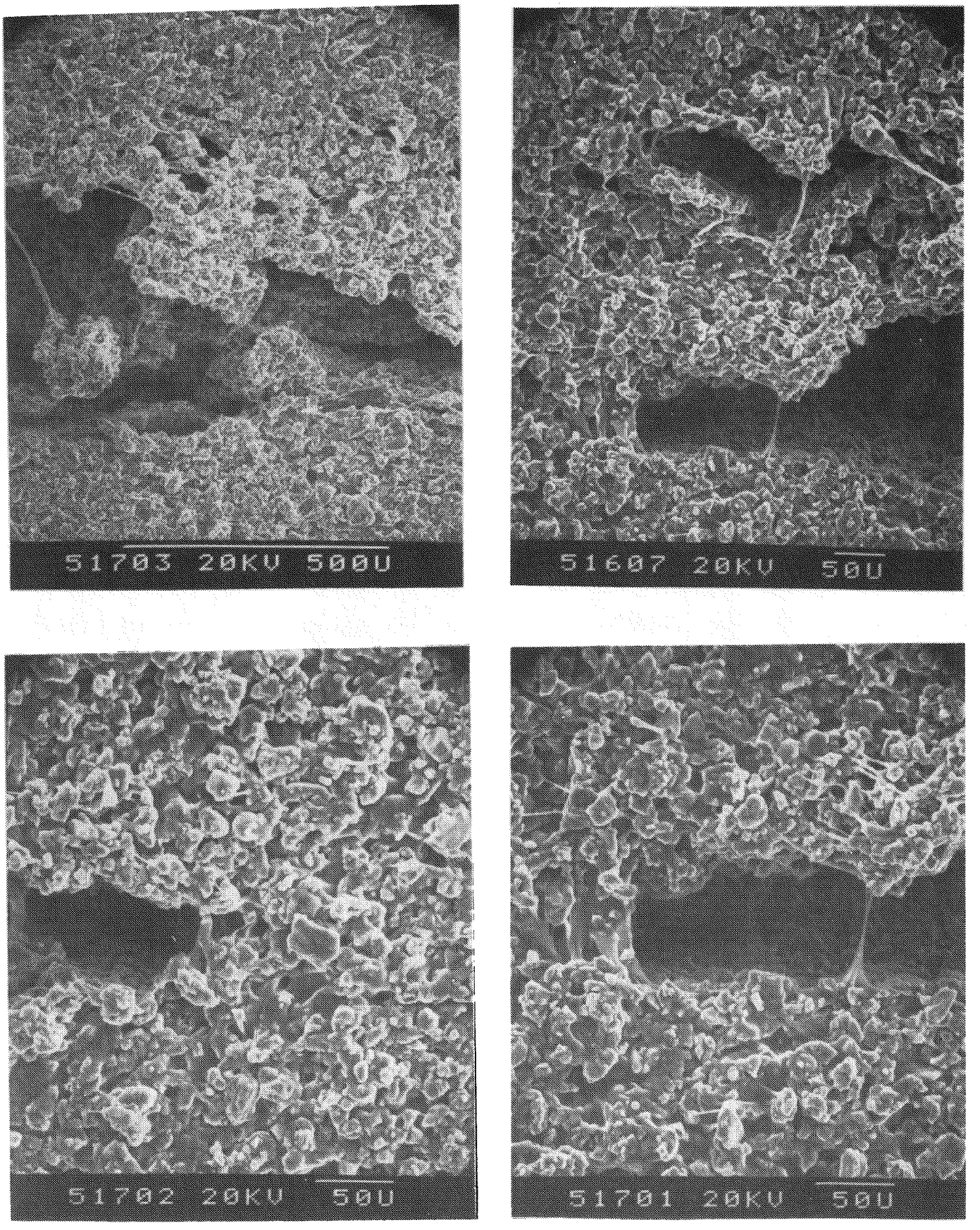


**Figure 17.** Scanning electron micrograph of UGS spall surface

## WAK-2

Spall shots were done on WAK-2 at impact pressures from 1.36 to 3.03 kbar. Figure 18 shows an example of the resultant particle velocity versus time plot for WAK-2 impacted by PMMA at a pressure of 1.36 kbar (projectile velocity of 76 m/s). The spall strength of WAK-2 calculated for this shot from Eq (2), with measured velocity pullback of 0.017 mm/μs, is 0.35 kbar (5000 psi). This result is given in Table 7 along with the spall strengths calculated from the data for the other spall tests. Table 7 also lists the particle velocities calculated from the Hugoniot data for the respective projectile velocities. These values doubled should agree with the measured free-surface velocities.

The data in Table 7 also indicate that a WAK-2 sample reacted upon being impacted by PMMA at 3 kbar. This result is to be compared with the result obtained in the reaction threshold tests where a WAK-2 sample impacted at the same velocity (0.15 mm/μs) but onto lithium fluoride to produce a higher impact stress (5.2 kbar) reacted briefly and then stopped.

Cross sections of the WAK-2 samples after the spall shots are shown in Figure 19. The spall planes are readily visible.

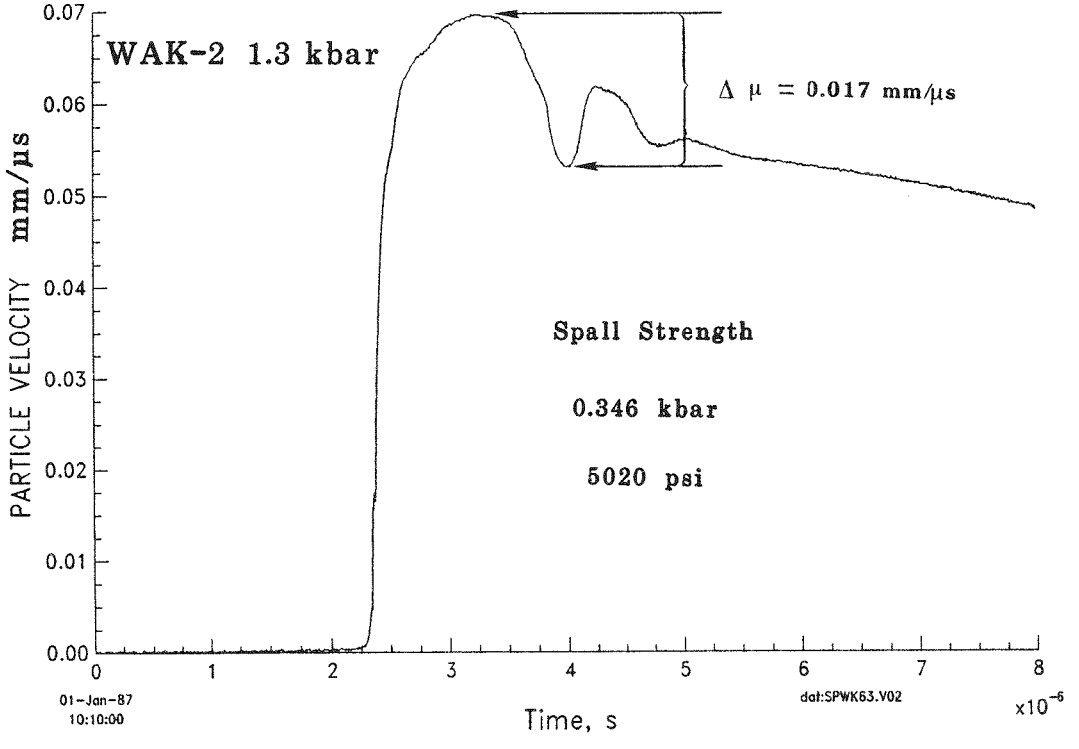


**Figure 18.** Particle velocity versus time record for PMMA impacting WAK-2 at 1.3 kbar

## Table 7. Spall results for WAK-2 propellant

| Projectile Velocity Measured (m/s) | Particle Velocity Calculated* (m/s) | X2 (m/s) | Free-Surface Velocity Measured (m/s) | Impact Stress Calculated | | Spall Strength Measured | |
|---|---|---|---|---|---|---|---|
| | | | | (kbar) | (ksi) | (kbar) | (ksi) |
| 76 | 32.4 | 64.8 | 70 | 1.36 | 19.72 | 0.346 | 5.02 |
| 115 | 49 | 98 | 101 | 2.10 | 30.45 | 0.315 | 4.57 |
| 163 | 69 | 138 | † | 3.03 | 43.94 | Reacted | |

*WAK-2:PMMA
†Trigger pin malfunctioned

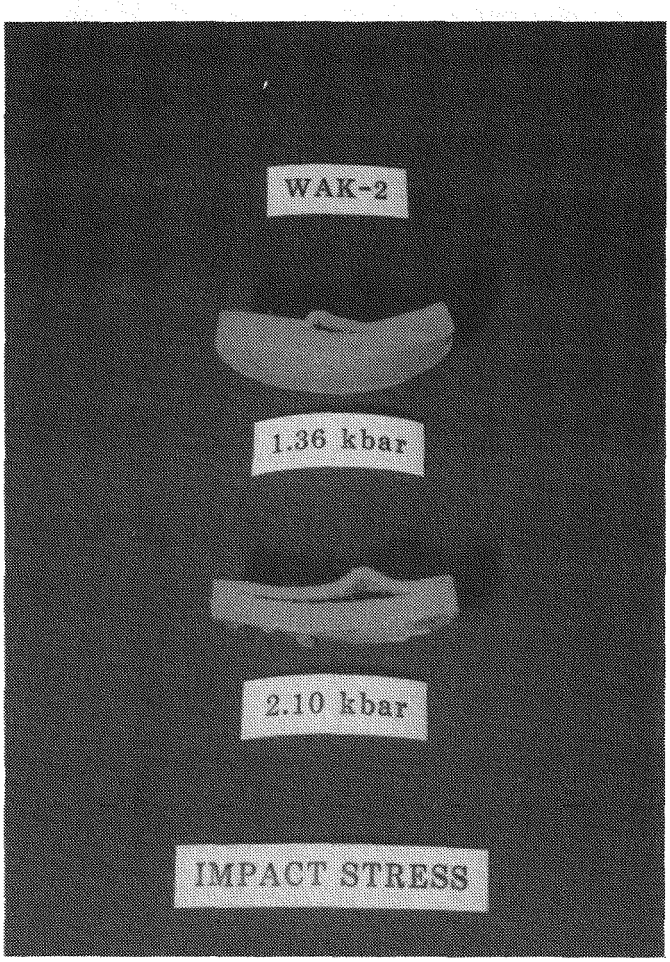


**Figure 19.** Photograph of WAK-2 samples after spall shots

# Discussion

## Hugoniot Measurements

The impact shots of WAK-2 propellant resulted in Hugoniot data which agreed with that supplied by the manufacturer, Morton-Thiokol. Using the values for initial density $\rho_o = 1.85$ g/cm$^3$, initial bulk sound velocity $C_o = 2.2$ mm/$\mu$s, and constant $S = 2.66$ in Eq (1) provides an accurate Hugoniot relation for this material for modeling. The impact shots of UGS simulant resulted in Hugoniot data that were within experimental measurement the same as that of WAK-2 for the range of pressures investigated. Thus, the UGS is acting as a good simulant for WAK-2 propellant with respect to shock properties.

## Reaction Threshold Measurements

The reaction threshold pressure for WAK-2 propellant was found to be ~3 kbar for the material dimensions and physical constraints of these tests. This reaction threshold pressure is in agreement in magnitude with values reported in the literature for energetic propellants. The study done at SRI International on VRA propellant found that an impact pressure of 6.3 kbar caused the propellant to burn.[5] The sample size was 50.8 mm diameter by 6.4 mm thick. Thus, a threshold value for WAK-2 of 3 kbar is in good agreement with results from SRI experiments, particularly for the larger size (50.8 mm diameter by 12.7 mm thick).

Table 8 gives the results for VXV, another energetic propellant of composition similar to that of WAK-2, from experiments done at LLNL.[4] The results showed that, for samples of dimensions 76 mm diameter by 76 mm long, an impact of 3.7 kbar produced a mild reaction, and an impact of 11.0 kbar caused a detonation after a 167-$\mu$s delay. Larger samples (152 mm diameter by 102-mm long) were found to detonate at lower impact pressures. A sample impacted at 8.6 kbar detonated. Since the objective of the LLNL study was primarily to determine the impact pressure at which a delayed detonation occurred, they did not investigate the lowest pressure at which a reaction was initiated. However, their finding that impacts at 3.7 and 8.6 kbar produced reactions and detonations agreed with the results from this study, where a 3-kbar impact produced a complete sample burn, and a 22-kbar impact produced a violent reaction that may have been a detonation.

**Table 8. Detonation results for VXV propellant***

| Target Dimensions | Projectile Dimensions | Impact Velocity (m/s) | Impact Pressure (kbar) | Results |
|---|---|---|---|---|
| 76-mm D | 156-mm D | 104 | 3.7 | Mild reaction |
| × 76-mm L | × 76-mm L | 150 | 5.6 | Mild reaction |
| | | 226 | 9.0 | Moderate reaction |
| | | 243 | 9.8 | Moderate reaction |
| | | 265 | 10.9 | Moderate reaction |
| | | 267 | 11.0 | Detonation 167 $\mu$s after impact |
| 152-mm D | 156-mm D | 196 | 7.6 | Mild reaction |
| × 102-mm L | × 76-mm L | 212 | 8.4 | Moderate reaction |
| | | 217 | 8.6 | Detonation 201 $\mu$s after impact |
| | | 235 | 9.4 | Detonation 209 $\mu$s after impact |
| | | 260 | 10.6 | Detonation 168 $\mu$s after impact |

*Ref. 2
D=Diameter
L=Length

## Spall Strength Measurements

The spall strengths of most materials (plastics, metals, ceramics, explosives) increase with increasing strain rate. Typically, the spall strength of a material increases from twofold to tenfold with an increase in strain rate from "static" ($10^{-3}$ $s^{-1}$) to "dynamic" ($>10^{+3}$ $s^{-1}$). The spall strength of the UGS simulant in this study increased from a static value of just above 0.011 kbar (158 psi) to about 0.22 kbar (3200 psi) under shock loading. This increase of twentyfold is above the expected increase range of tenfold of this material. Table 9 lists the tensile and spall strengths for individual materials of interest in this study for which data were available. The magnitude of the relative strength values suggests that the strength of UGS could be a result of fracture of one or more materials in the composite and separation between boundaries of other constituents of the composite along the fracture plane. One possibility is that the fracture plane goes predominantly through the $NaSO_4$. This could occur both because the strength of $NaSO_4$ is low and because it is the major constituent. However, $NaSO_4$ exists as individual crystals within the composite and does not form a continuum. Thus, a fracture through this material would also have to propagate through another material. Since the DBP and HDAP are the continuum that binds the composite together, the fracture plane must include these materials.

A second possibility for fracture takes into account the very weak bonding between the polymer binders and sodium sulfate and aluminum particles. In this fracture hypothesis, the crack propagates along the $NaSO_4$-polymer and Al-polymer boundaries, causing a separation at these locations, and then propagates across the polymers along the fracture plane. This phenomenon is called "dewetting" and occurs in all composite solid propellants to some extent when a load is applied.[20] The relative motion of particles imbedded in the matrix produces sufficiently high stresses near the binder-filler interfaces to cause rupture, and the binder-filler bonds may be pulled loose. As dewetting takes place, the reinforcing effects of the filler are reduced, and a decreasing modulus of elasticity results. Any continued deformation, such as tearing, is sustained by the binder until the sample breaks or spalls. This fracture hypothesis was proven for the case of a composite propellant and its simulant.[1]

Figure 17, a micrograph of a fracture in UGS, confirms this second hypothesis for this material. The fracture runs alongside the $NaSO_4$ crystals and Al spheres, at the bond planes between them and the polymers, and through the connecting polymers. The fracture strength is reflected in the stress needed to fracture the proportion of polymer binder between the solid fillers, $NaSO_4$ crystals and Al particles.

Similar results have been found for the WAK-2 propellant. The tensile strength was reported to be near 0.007 kbar (100 psi);[9] the spall strength was 0.33 kbar (4785). A factor of almost 50 increase in spall strength over tensile strength is higher than the expected tenfold increase. However, the same arguments can be used for the fracture of WAK-2 as were used for the fracture of UGS. The spall is a result of the fracture of the double-base propellant, and the strength is approximately proportional to the volume percentage of polymer-binder material, namely the nitrocellulose, in the propellant.

In addition, SRI studies of VRA found that the dynamic tensile strength was near 0.1 kbar (1500 psi), a factor of 15 higher than the static tensile strength.[5] Therefore, a spall strength of 0.33 kbar measured on WAK-2, a similar propellant, is in good agreement with these dynamic tensile strength values.

Results from the SRI study also indicated that an impact stress of ~1.6 kbar was necessary to produce a visible spall plane in a sample. This result agrees with results from this study as well as the previous study on a composite propellant and its simulant.[1] However, the previous study demonstrated that a spall plane may form in the sample at lower impact stresses, but that it is necessary to use a microscope at 100X to see the fracture. In addition, the value of spall strength is more properly calculated from "pullback" measurements, and these values are typically about a factor of 5 lower than the values obtained from visible fracture at threshold impact stresses. Since the measured free-surface velocity was very close to twice the particle velocity calculated from the Hugoniot relationship, there was very little attenuation of the shock intensity in these materials at these shock levels. Thus, the impact stress, peak tensile stress, fracture stress, and spall strength would all be essentially the same value for a sample shocked just enough to induce incipient spall.

**Table 9. Tensile and spall strengths of selected materials**

| Material | Tensile Strength (kbar) | Tensile Strength (psi) | Reference No. | Spall Strength (kbar) | Spall Strength (psi) | Reference No. |
|---|---|---|---|---|---|---|
| Aluminum | 0.900 | 13000 | 14 | 10.00 | 145000 | 15 |
| Sodium Sulfate | 0.015* | 217* | 16 | 0.40* | 5800* | 17 |
| UGS | 0.011 | 158 | 9 | 0.22 | 3190 | |
| HMX | 0.031 | 450 | 18 | ? | ? | 19 |
| WAK-2 | 0.007 | 100 | 9 | 0.33 | 4785 | |

*Estimated value from data for similar salts

The *incipient* spall strength or "pullback" strength is a dynamic, ultimate tensile strength value analogous to the standard, static, ultimate tensile strength value. The latter value is recognized by the materials community as a property of the material and is not geometry dependent. However, from a lethality viewpoint, the tensile stress required to form a complete, visible spall plane may be more important. This value would be ~1.5 to 2.0 kbar for these tests, but is highly dependent upon the geometry of the sample and test fixturing. The *complete* spall strength is a dynamic fracture strength value analogous to a static fracture strength value. This value is not recognized by the materials community as a property of the material because it is very geometry dependent.

Finally, observations on the fracture morphology of VRA propellant at SRI showed that fracture was initiating both within HMX grains and at the HMX-matrix interface and then propagating across the double-base propellant matrix. This result agrees with the observations of this study. The spall strength is primarily a result of fracture across the double-base propellant matrix.

The spall strengths measured for the energetic propellant WAK-2 and its simulant UGS in this study (0.33 and 0.22 kbar, respectively) are somewhat higher than those found for the composite propellant TP-H1207C and its simulant H-19 (0.25 and 0.18 kbar, respectively) in the previous study. This relationship is in agreement with the finding that the spall strength is proportional to the amount of polymer binder in the formulation. The energetic propellant and its simulant have proportionately more organic materials acting as a binder than the composite propellant and its simulant. Also, all of the materials had similar fracture characteristics.

# Summary

Hugoniot data obtained on a few samples of both WAK-2 and UGS resulted in Hugoniot parameters that matched those for WAK-2 provided by the manufacturer of the materials, Morton-Thiokol, Inc. Shock experiments on WAK-2 indicated that the impact pressure for initiation of a reaction is around 3 kbar. WAK-2 impacted at 22 kbar may have detonated. The spall strengths of WAK-2 and UGS were found to be 0.33 and 0.22 kbar, respectively. The crack path of the spall plane was found to go through the polymer binder materials such as HDAP and DBP and around the inorganic fillers such as $NaSO_4$ and Al. The spall strengths were found to be proportional to the volume fraction of the polymer.

Currently, attenuation experiments are being done on both the composite propellant TP-H1207C and its simulant H-19 and the energetic propellant WAK-2 and its simulant UGS to obtain attenuation values to be used in material modeling for a one-dimensional, finite-difference wave propagation code named WONDY.

# References


[1]L. J. Weirick and D. W. Dugan, *Characterization of Morton-Thiokol Booster-Rocket Propellant TP-H1207C and Its Simulant H-19*, SAND88-0930 (Albuquerque, NM: Sandia National Laboratories, December 1988).

[2]L. R. Green, E. James, E. Lee, E. Nidick, and E. Chambers, *Air Force Propellant Study*, UCID 19041 (Livermore, CA: Lawrence Livermore National Laboratory, May 1981).

[3]P. Urtiew, E. James, and K. Scribner, *High Energy Propellant Safety (HEPS) Program. Highlights, Volume I*, UCID 17272-79-3 (Livermore CA: Lawrence Livermore National Laboratory, 1979).

[4]L. Green, E. Chambers, E. James, E. Lee, and A. Weston, *Summary Report on Experimental Work Using the 155-mm Gun*, UCID 19424 (Livermore CA: Lawrence Livermore National Laboratory, June 1982).

[5]W. J. Murri, Y. Horie, and D. R. Curran, *Dynamic Fracture Experiments on VRA Propellant*, UCRL-15550 (Livermore, CA: Lawrence Livermore National Laboratory, June 1977).

[6]C. S. Speight, "Observation of Spallation and Attenuation Effects in Aluminum from Free-Surface Velocity Measurements," Foulness Division Note FDN 4/71 (Aldermaston, England: Atomic Weapons Research Establishment, 1971).

[7]W. M. Isbell and D. R. Christman, "Shock Propagation and Fracture in 6061-T6 Aluminum from Wave Profile Measurements," MSL-69-60 (Detroit, MI: Materials and Structures Laboratory, General Motors Corp., 1970).

[8]D. R. Christman, W. M. Isbell, and S. G. Babcock, "Measurements of Dynamic Properties of Materials, Vol. V, OFHC Copper," MSL-70-23 (Detroit, MI: Materials and Structures Laboratory, General Motors Corp., 1971).

[9]Memo dated 12 October 1987, to: L. W. Poulter, from: W. F. Dunn, "Extended Ambient Cure of H-19 Propellant" (Brigham City, UT: Morton-Thiokol Inc., Wasatch Operations).

[10]S. A. Sheffield and D. W. Dugan, "Description of a New 63-mm Diameter Gas Gun Facility," *Shock Waves in Condensed Matter*, ed. Y.M. Gupta, Plenum Press (1986).

[11]L. M. Barker and R. E. Hollenbach, "Laser Interferometer for Measuring High Velocities of Any Reflecting Surface," *J Appl Phys* 43:11 (Nov 1972).

[12]W. F. Hemsing, "Velocity Sensing Interferometer (VISAR) Modification," *Rev Sci Instrum* 50:1 (Jan 1979).

[13]O. B. Crump, Jr., and P. L. Stanton, *Push-Pull, Double-Delay-Leg or Dual VISAR*, SAND87-1974 (Albuquerque, NM: Sandia National Laboratories, Dec 1987).

[14]"Metals, Plastics, Elastomers & Other Engineering Materials," *Machine Design* (March 1978).

[15]L. Davison and R. A. Graham, "Shock Compression of Solids," *Physics Reports, Review Section of Physics Letters*, V55, No. 4 (New York: IEEE, 1979).

[16]F. D. Hansen, K. D. Mellegard, and P. E. Senseny, "Elasticity and Strength of Ten Natural Rock Salts," *The Mechanical Behavior of Salt*, eds. H. R. Hardy, Jr., and M. Langer, (Clausthal, Germany: Trans Tech Publishing, 1984).

[17]D. E. Grady, private communication (Albuquerque, NM: Sandia National Laboratories, August 1988).

[18]G. Poulain, "Behavior of HMX, TATB Compositions under Mechanical Loading," DEA Physics of Explosives Mtg. (Los Alamos, NM: Los Alamos National Laboratory, April 4-6, 1989).

[19]C. Loupias, private communication (Gramat, France: Centre d'Etudes de Gramat, April 6, 1989).

[20]F. N. Kelly, "Solid Propellant Mechanical Property Testing, Failure Criteria, and Aging," *Propellants Manufacture, Hazards, and Testing*, eds. C. Boyers and K. Klager (Washington, DC: American Chemical Society, 1969).

DISTRIBUTION:

3 Defense Nuclear Agency
Attn: Dr. M. Frankel, SPWE
Maj. R.D. Yoho, PRPD
Capt. P.J. Wolf, SPWE
6801 Telegraph Road
Alexandria, VA 22310-3398

1 Aerojet Solid Propulsion Co.
Attn: G. Etzel, Bldg. 1960, D2335
P.O. Box 15699C
Sacramento, CA 95813

1 Aerospace Corporation
Attn: H. Blaes
P.O. Box 92957
Los Angeles, CA 90009-2957

1 Air Force Weapons Laboratory
Attn: Lt. Col. C. Nefzger
Kirtland AFB, NM 87117-6008

2 APTEK
Attn: S.H. Sutherland
T. Duffey
1257 Lake Plaza Drive
Colorado Springs, CO 80906-3578

3 APTEK
Attn: H. Lindberg
L. Schwer
Y. Murray
4320 Stevens Creek Blvd.
Suite 195
San Jose, CA 95129

1 Astronautics
Attn: W.W. Wells
AFAL/RKB
Edwards AFB, CA 93523

1 Defense Advanced Research Projects
Attn: F. Patten
1400 Wilson Blvd.
Arlington, VA 22209-2308

2 General Research Corporation
Attn: R. Globus
W. Naumann
P.O. Box 6770
Santa Barbara, CA 93160-6770

1 Hercules Inc.
Attn: S. Beckwith
Magna, UT 84044

1 JAYCOR
Attn: M. Treadaway
P.O. Box 85154
San Diego, CA 92138

1 Johns Hopkins University
Attn: Ms. K. Strange
Applied Physics Laboratory
CPIA Laurel, MD 20707-6099

1 DETIR
Attn: R. Harter
Kaman Sciences Corporation
Tempo Division
2560 Huntington Ave. Suite 500
Alexandria, VA 22303-1490

1 DETIR
Kaman Sciences Corporation
816 State Street
P.O. Drawer QQ
Santa Barbara, CA 93102-1479

4 K-Tech Corporation
Attn: L. Lee
T. Smith
A. Greb
E. Smith
901 Pennsylvania Ave. N.E.
Albuquerque, NM 87110

3 McDonnell Douglas Astronautics Co.
Attn: J.S. Kirby, A3-365 (13-3)
D.L. Johnson, A3-365 (13-3)
L.E. Thompson, A3-365 (13-3)
5301 Bolsa Avenue
Huntington Beach, CA 92647

1 Mission Research Corporation
Attn: S. Stone
Bldg. H
3505 Cadillac Avenue
Costa Mesa, CA 92626

DISTRIBUTION: (continued)

3 Morton Thiokol
Attn: L.D. Ericksen, R-11
R.D. Taylor
E. Wolcott
Wasatch Operations
P.O. Box 524
Brigham City, UT 84302

1 Office of Military Applications
Attn: Maj. Ross Lushbough/DOE
DP 255 GTN
Washington, DC 20545

1 R & D Associates
Attn: R. Gould
P.O. Box 9695
Marina del Rey, CA 90291

2 S-Cubed
Attn: J. Gurtman
J. Tripplett
Box 1620
La Joya, CA 92038-1620

4 SRI International
Attn: B.S. Holmes
J. Gran
D. Curran
W.J. Murri
333 Ravenswood Ave.
Menlo Park, CA 94025-3493

3 Los Alamos National Laboratory
Attn: R.S. Thurston, WX4
C.E. Morris, J970
R.S. Dingus, E531
P.O. Box 1663
Los Alamos, NM 87545

8 Lawrence Livermore National Laboratory
Attn: A.L. Austin, L-47
H.W. Kruger, L-84
M. Gerassimenko, L-84
F. Serduke, L-84
D.A. Schauer, L-122
S.J. Sackett, L-122
E.L. Lee, L-368
L.G. Green, L-368
P.O. Box 808
Livermore, CA 94550

| | | |
|---|---|---|
| 1 | 1230 | J.E. Powell |
| 1 | 1273 | M.K. Matzen |
| 1 | 1530 | D.B. Hayes |
| 1 | 1533 | M.E. Kipp |
| 1 | 1534 | J.R. Asay |
| 1 | 1534 | L.C. Chhabildas |
| 1 | 1550 | C.W. Peterson, Jr. |
| 1 | 2500 | R.L. Schwoebel |
| 1 | 2510 | D.H. Anderson |
| 1 | 2512 | J.G. Harlan |
| 1 | 2512 | R.G. Jungst |
| 1 | 2512 | W.W. Tarbell |
| 1 | 2513 | D.E. Mitchell |
| 1 | 2514 | L.L. Bonzon |
| 1 | 2514 | D.W. Dugan |
| 1 | 2514 | L.M. Moore |
| 1 | 2514 | P.L. Stanton |
| 10 | 2514 | L.J. Weirick |
| 1 | 2515 | P.D. Wilcox |
| 1 | 2515 | V.M. Loyola |
| 1 | 2515 | A.M. Renlund |
| 1 | 5166 | R.E. Setchell |
| 1 | 7530 | T.L. Workman |
| 1 | 7533 | R.A. Benham |
| 1 | 8200 | R.J. Detry |
| 1 | 8240 | C.W. Robinson |
| 1 | 8242 | M.R. Birnbaum |
| 1 | 8242 | B.L. Kistler |
| 1 | 8242 | A. McDonald |
| 1 | 8242 | L.I. Weingarten |
| 1 | 8431 | L.A. West |
| 1 | 8524 | J. A. Wackerly |
| 5 | 3141 | S.A. Landenberger |
| 8 | 3141-1 | C L. Ward<br>For DOE/OSTI |
| 3 | 3151 | W.I. Klein |